Journal of Polymers and the Environment
https://doi.org/10.1007/s10924-023-03180-7

ORIGINAL PAPER

Novel Fluoroboric Acid Additive for Blend Membrane to be Used in PEM Fuel Cell, Characterization Studies, and Performance Test

Yavuz Yagizatli[1,2] · **Irfan Ar**[1]

Accepted: 30 December 2023

Abstract

This study focuses on developing an alternative membrane for PEMFC due to the disadvantages of using Nafion. Fluoroboric acid (FBA) was used as an additive material to SPEEK-PVA blend membranes at different weight ratios (1%, 5%, 7.5%, 10%, and 12.5%), and a synthesis procedure was carried out with the solution-casting. Thermal crosslinking was performed with all membranes. Utilizing FBA, with its highly electronegative fluorine groups, is a novel approach expected to enhance proton conductivity. The structural, morphological, and thermal properties of the synthesized membranes were determined by FTIR, XRD, SEM, TGA-DTG, and DSC. Water uptake capacity (WUC), swelling property, area change, dynamic mechanical analysis, ion exchange capacity (IEC), AC impedance analysis, hydrolytic stability, and oxidative stability analyses were performed for fuel cell applications. Although FBA does not have a crystal structure, the synergy it created with the SPEEK-PVA membrane increased the crystallinity of the membrane and, accordingly, glass transition temperature. SEM images of membranes at a ratio above 7.5% show that agglomerations occur in the structure and this is supported by other analyses. It was determined that the membrane composition with the highest WUC (16.44%), IEC (1.55 meq/g), and proton conductivity (0.57 S/cm) values contained 7.5% FBA from the characterization studies, and a single-cell performance test was actualized with this. 418 mA/cm^2 current density and 250.8 mW/cm^2 power density were obtained at 0.6 V cell potential, with the membrane containing 7.5% FBA. This study shows that the synthesized membrane, especially the FBA, is a promising option for PEMFC application.

✉ Yavuz Yagizatli
yavuzyagizatli@gazi.edu.tr

[1] Department of Chemical Engineering, Faculty of Engineering, Graduate School of Natural and Applied Sciences, Gazi University, Eti Mahallesi, Yükseliş Sokak, No:5, Maltepe, 06570 Ankara, Turkey

[2] Department of Chemical Engineering, Gazi University Engineering Faculty, Room 544, Maltepe, 06570 Ankara, Turkey

Published online: 01 February 2024

Graphical Abstract

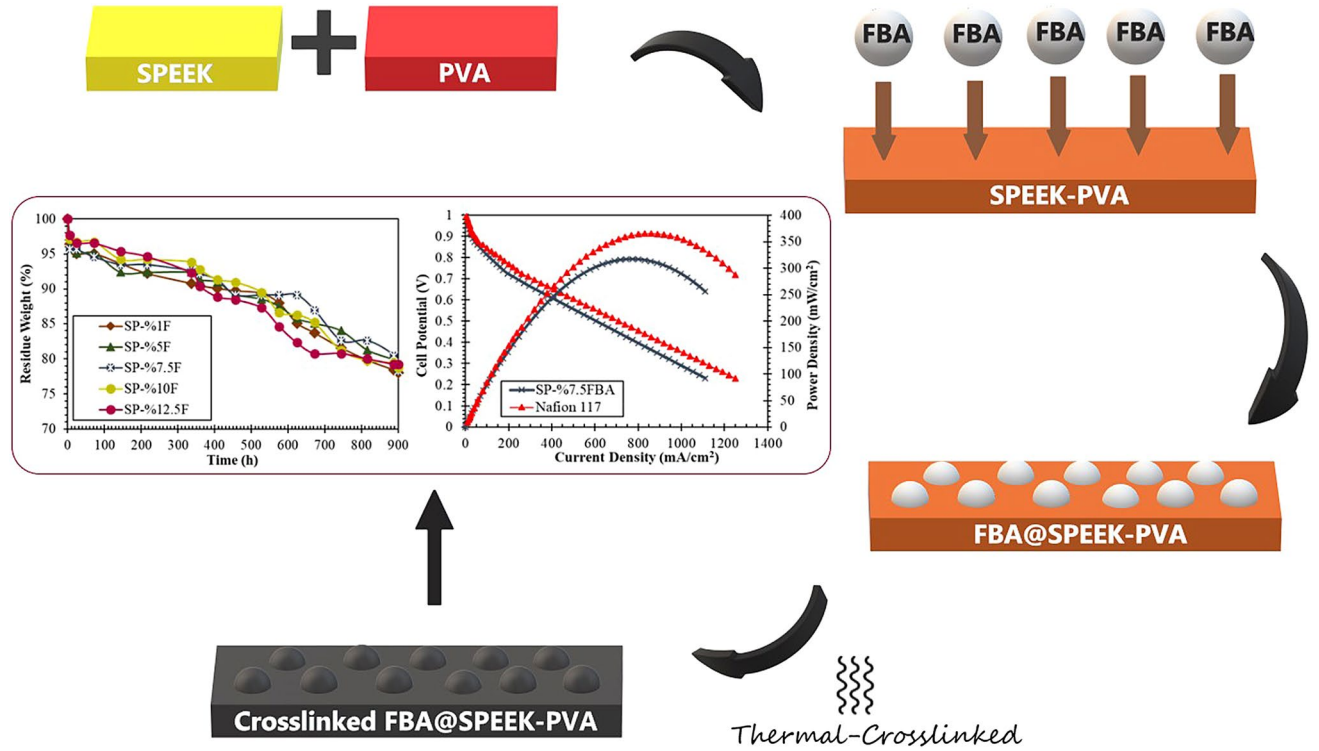

Keywords Fluoroboric acid · PEMFC · Fuel cell performance · SPEEK · PVA

Introduction

In the present day, there is a widespread global preference for sustainable energy sources to preserve the environment. This stems from the acknowledgment of the limited reservoirs of fossil fuels for future use, coupled with the imperative to mitigate CO_2 emissions, a direct contributor to the issue of global warming [1–3]. In light of these challenges, numerous research cohorts propose that Fuel Cells (FC) are emerging as the foremost and environmentally friendly alternative for energy conversion. FCs are electrochemical power sources that convert chemical reaction energy directly into electrical energy, have high energy efficiency, zero emission, do not cause environmental or noise pollution, and will be used at much greater intensity and scale in the near future [4–7]. FCs are clean energy technologies that can meet increasing energy demands today and in the future [8–10]. Proton exchange membrane fuel cell (PEMFC) is the type of fuel cell that is most commercially and widely used today, with its advantages and potential compared to other types [11, 12]. . The wide power range, easy scalability, low-temperature operation, short startup time, the solid polymer electrolyte used reduces corrosion and facilitates electrolyte management, and high power density are the main advantages that make PEMFC stand out [13–15]. High power density and fast startup time make PEMFC competitive in the automotive industry, and low operating temperature in technology and transportation applications such as laptops and mobile phones [16].

The electrolyte is an essential and notable PEMFC component, consisting primarily of a polymer structure designed to transport hydrogen ions and provide high proton conductivity effectively [17–19]. The electrolyte membrane employed in PEMFC serves three distinct purposes: facilitating proton transport from the anode to the cathode, dividing reactant gases, and delivering electrical isolation to prevent electron passage through the membrane [20–22]. Currently, Nafion is the most commonly utilized and referenced membrane in PEMFC. However, ongoing efforts to find alternative membranes persist because of Nafion's drawbacks, which include its high cost, significant fuel permeability, and reduced proton conductivity under high-temperature and low-humidity conditions [15, 23, 24]. An alternative to Nafion as a membrane should be cost-effective, durable, exhibit high proton conductivity, possess minimal fuel permeability, offer strong thermal, chemical, oxidative, and mechanical resistance, have low susceptibility to water, and be suitable for operation across various conditions [25–27].

The membrane matrix in polymer blend membranes, a type utilized as proton exchange membranes, comprises a minimum of two distinct polymers to amalgamate the advantageous characteristics of the polymers into a unified structure while mitigating their respective shortcomings. Many different polymers such as sulfonated poly ether ether ketone (SPEEK) [28, 29], polyvinyl alcohol (PVA) [30, 31], sulfonated poly arylene ether solfone (SPEAS) [32, 33], poly ether sulfone (PES) [34, 35], polybenzimidazole (PBI) [36, 37] etc. can be used in the membrane matrix. SPEEK exhibits its variable proton conductivity and strong thermal-chemical stability, which can be adjusted according to the degree of sulfonation [38, 39]. As the degree of sulfonation increases, there is an increase in proton conductivity in SPEEK; however, this improvement is accompanied by a decline in the membrane's mechanical properties. Excessive swelling and long-term stability issues initiated by hydroxyl radicals can compromise the mechanical integrity of the membrane. Blend membrane formation, and using affective additive materials is an effective solution to address these challenges and enhance proton conductivity in SPEEK without sacrificing its mechanical properties. PVA, which, on its own, cannot serve as a membrane due to its low proton conductivity and susceptibility to water solubility, is frequently incorporated into blend membranes owing to its high hydrophilicity, excellent film-forming attributes, and strong chemical and mechanical properties [40, 41]. Fabricating a SPEEK-PVA blend membrane enhances its mechanical properties. The mechanical properties of SPEEK, such as elongation at break, maximum tensile strength, and Young's modulus, deteriorate as the degree of sulfonation increases. However, the good mechanical properties of PVA improve the deteriorating mechanical properties of SPEEK in the formation of a blended membrane with SPEEK [42–45]. . However, the proton conductivity decreases compared to the pristine SPEEK membrane due to the reduction of active sulfonic acid groups in the structure with the SPEEK-PVA blend membrane. The properties of the membrane can be fine-tuned to specific requirements using appropriate additives.

Many additives such as graphene oxide (GO) [46, 47], titanium dioxide (TiO_2) [48, 49], tetraethyl orthosilicate (TEOS) [18, 50], boron phosphate (BP) [29, 51], zirconium phosphate (ZrP) [52, 53], zirconium oxide (ZrO) [54, 55], silica [56, 57] etc. have been used in synthesized membranes for PEMFC. These additives are incorporated to enhance the membrane's weaknesses. In a study using GO additive, Rambabu et al. stated that GO additive increased the proton conductivity of the membrane and reduced fuel permeability. However, the membrane's flexibility and mechanical strength decreased [46]. It has been reported that the ZrO additive significantly increases the mechanical strength of the polymer membrane [58]. In a study in which TiO_2 additive was used, they stated that the fuel cell performance of the membrane increased with the additive material and that TiO_2 additive had a positive effect on proton conductivity [48]. Cali et al. stated that the BP additive increased the proton conductivity and mechanical strength of the SPEAK/PVDF blend membrane [29]. As a result of the research, it has been determined that the use of boron-based additive materials in PEMs is a very promising option.

In this study, fluoroboric acid (FBA), which has not been used before in the literature, was used as an effective additive material. FBA additive is the novelty aspect of this study. Its use in fuel cells and its morphological, physical, and chemical effects on the blend membrane will be a first in the literature. SPEEK and PVA were used as the membrane matrix, which creates a good synergy between them. It is thought that the proton conductivity, which decreases with the blend membrane, can be improved by fluoroboric acid additive. In particular, it is predicted that fluorine, which is in the FBA structure and has high electronegativity, will play a leading role in increasing proton conductivity [59]. In our prior research, we observed that the SPEEK-PVA blend membrane exhibited partial dissolution in water. To mitigate this issue, a thermal crosslinking process was employed for all the membranes synthesized in our study [40]. Fourier transform infrared (FTIR), X-ray diffraction (XRD), thermal gravimetric analysis (TGA-DTG), differential scanning calorimetry (DSC), scanning electron microscope (SEM), water uptake capacity (WUC), swelling properties (SP), change in size, ion exchange capacity (IEC), dynamic mechanical analysis (DMA), hydrolytic stability, oxidative stability, and AC impedance analyzes were performed with the synthesized membranes. At the end of the study, single cell performance tests were carried out with the most suitable membrane compositions at 80°C and 100% relative humidity.

Materials and Methods

Polyoxy-1, 4-phenyleneoxy-1,4-phenylenecarbonyl-1, 4-phenylene (PEEK, Aldrich, M_w: 20.800) and polyvinyl alcohol (PVA, Aldrich, 99%, M_w: 85,000–124,000) as membrane matrix. Sulfuric acid (H_2SO_4, Aldrich, 96%) as sulfonation agent. Fluoroboric acid (HBF_4, Honeywell, 50%) as additive. Dimethyl sulfoxide (DMSO, Sigma-Aldrich, > 99%) as solvent. Hydrogen peroxide (H_2O_2, Sigma-Aldrich, 30%) and iron (II) sulfate hydrate ($Fe_SO_4.7H_2O$, Sigma-Aldrich, BioReagent) as Fenton agents.

Obtaining SPEEK by PEEK Sulfonation

The SPEEK was achieved through the sulfonation of PEEK. The sulfonation process was conducted for 315 min at a temperature of 50 °C. Prior to sulfonation, PEEK pellets were dried and stirred in concentrated sulfuric acid at a

concentration of 20% (w/v) for the specified duration and temperature. Following the stirring, the solution was poured into an ice-filled beaker to form a solid strip, effectively terminating the sulfonation reaction by lowering the temperature to below 10 °C. The SPEEK strips, which transitioned from red to white in the ice bath, were rinsed with deionized water until the pH reached a range of 6–7. The resulting neutral SPEEK strips were subsequently dried in an oven at 60 °C. The sulfonation degree of SPEEK polymer was determined as 56.98%.

FBA-additive Blend Membrane Synthesis

SPEEK and PVA polymers, in a weight ratio of 85–15%, were individually mixed in separate 5% (w/v) DMSO solutions at 80 °C using a magnetic stirrer. The PVA solution was gradually introduced into the SPEEK solution, and the combined mixture was stirred with a magnetic stirrer at 80 °C for 24 h until it reached a homogenized state. After achieving homogeneity, the FBA additive was incorporated into the solution at specified weight ratios, and the mixture was stirred for at least 3h. The resulting homogenized solution was poured into Petri dishes and left to dry in an oven. Finally, the dried membranes underwent thermal crosslinking, placing the membranes between two glass plates at 180 °C for 48 h in an oven. The thermal crosslinking process was carried out to prevent the partial dissolution of the synthesized membrane in water. Since the membrane will be in constant contact with water in the fuel cell, partial dissolution of the membrane in water is unacceptable. For this reason, as a result of the thermal crosslinking process carried out with different procedures found in the literature, the thermal crosslinking process was carried out for 48 h at 180 °C, which prevents weight loss the most. The thermal crosslinking process and weight losses performed with the synthesis membrane at different temperatures and times are given in Table 1.

For a schematic representation of the FBA-additive blend membrane synthesis process, please refer to Fig. 1.

Example nomenclature of synthesised membranes;

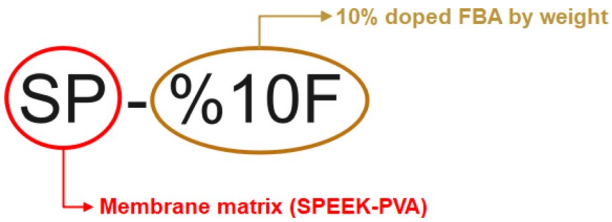

The possible planar structure of the FBA-additive SPEEK-PVA blend membrane, synthesized by the solution casting method and obtained as a result of the thermal crosslinking process carried out at 180 °C for 48 h, is given in Fig. 2.

Table 1 Weight losses as a result of different thermal crosslinking procedures applied to the synthesized membrane

Membrane	Thermal crosslinking conditions	Weight loss (%) for 24 h	
		20 °C	80 °C
SP-%10FBA	without thermal crosslinking	23.6%	24.7%
	120 °C, 3 h [60]	18.8%	21.4%
	180 °C, 2 h [61]	9.8%	13.8%
	180 °C, 48 h [62]	3.9%	4.8%

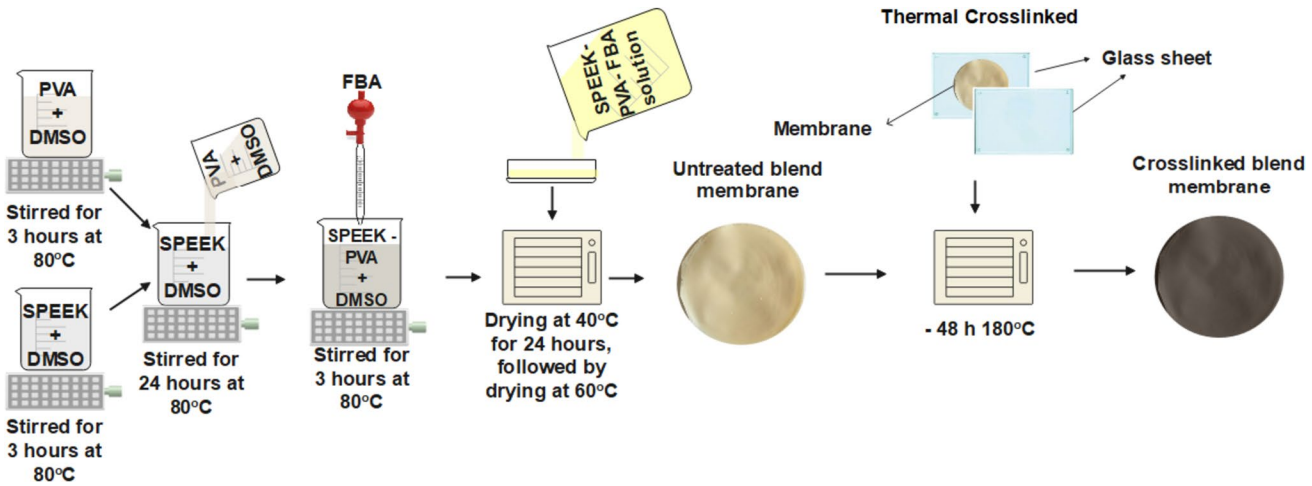

Fig. 1 Schematic representation of FBA-additive blend membrane synthesis

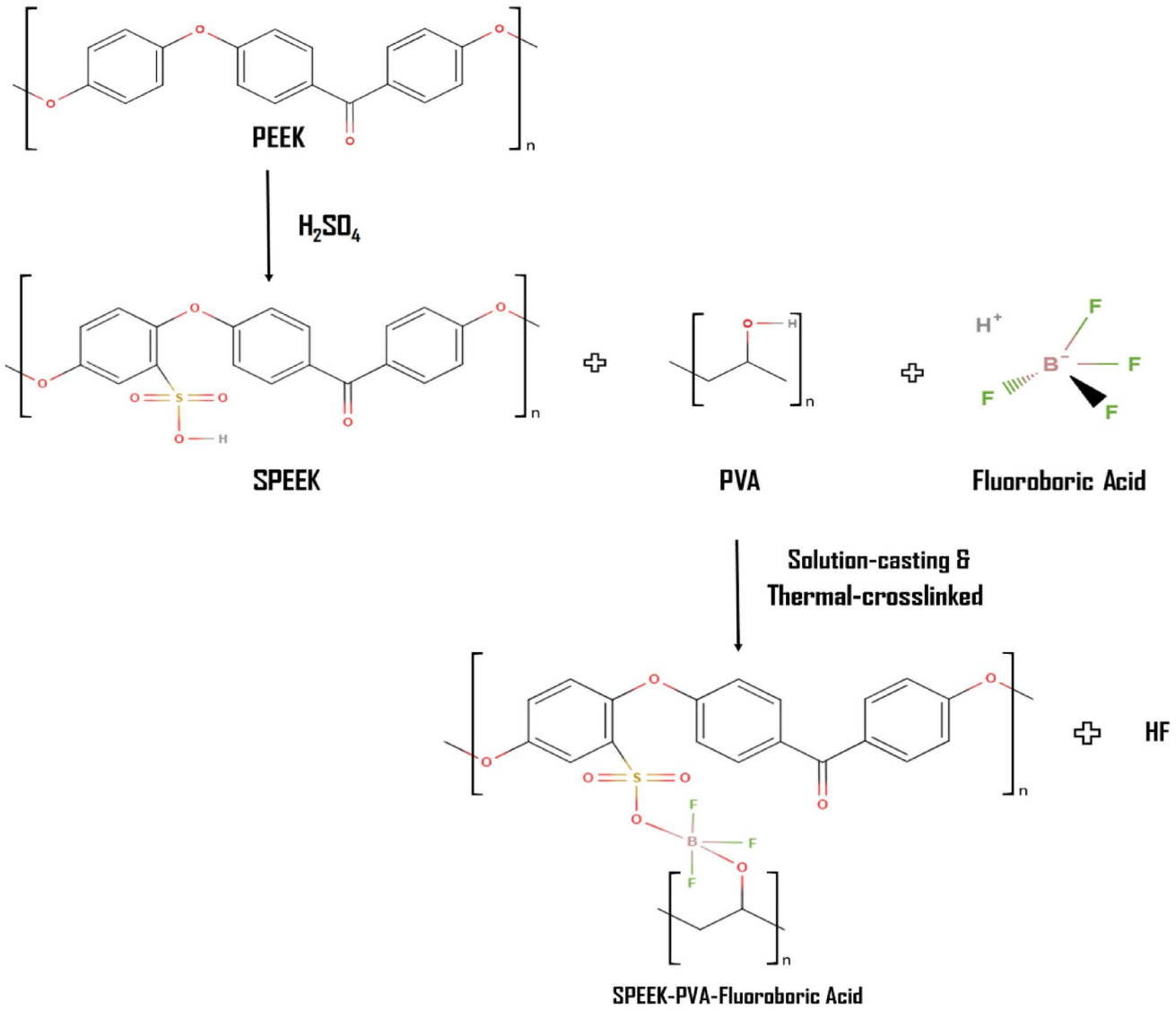

Fig. 2 Possible FBA-additive SPEEK-PVA blend membrane planar structure and reaction scheme

Characterization Studies of Membranes

FTIR analyses were conducted to identify the chemical bonds formed within the synthesized membrane structure and to assess its structural properties. FTIR analyses were carried out using a Bruker Vertex FTIR spectrophotometer in the wavenumber range of 400–4000 cm^{-1}. These analyses utilized an ATR measuring apparatus and a DT-GS detector. XRD analyses were carried out to assess the amorphous/crystalline phases, crystal size, and the success of membrane synthesis. XRD was performed using the Rigaku D/MAX 2200 instrument (scan range:1-90°, scan speed: 2°/min). TGA-DTG analyses were performed to evaluate the synthesized membranes' thermal stability and determine weight losses with temperature. These analyses were conducted using the Setaram Labsys systems (temperature range: 30–900 °C, heating rate 10 °C/min). DSC analyses were carried out using the Perkin Elmer Diamond Differential Scanning Calorimeter (temperature: 20-350°C, heating rate: 10°C/min). These analyses aimed to investigate the behavior of the membranes during heating and/or cooling and to identify glass transition temperatures that impact proton conductivity. Following the synthesis of the blend membrane, SEM analyses were conducted to examine changes on the membrane surface after adding FBA and assess the synthesis's success. SEM analyses were performed using the QUANTA 400 F Field Emission SEM device at three different magnifications (x20000, x50000, and x100000). Before SEM measurement, the membranes were soaked and broken in a liquid nitrogen environment,

the gold coating was applied to the surface of the membranes, and cross-sectional area imaging was performed from the broken interface.

For WUC, SP, and change in size measurements, critical parameters influencing membrane performance, the membranes were dried in an oven to remove moisture. Subsequently, the dried membranes were weighed on a precision balance. Their thickness was measured from 15 different points using a SHEEN brand thickness gauge, the average thickness value was used in the calculations, and their dimensions were determined with digital calipers. The average thickness of the synthesized membranes was measured at 96.17 ± 6.35, 104.09 ± 7.48, 109.14 ± 8.93, 100 ± 12.45, and 90 ± 14.73, respectively, from 1% FBA additives to 12.5% FBA additives by weight in the line with increasing FBA content. The membranes were submerged in DI water at various temperature conditions for one day. Excess water was removed from the soaked membranes, and weighing, thickness, and size measurements were repeated. WUC, SP, and size change measurements were repeated three times, and the results obtained were averaged for three repetitions. Utilizing the data obtained, the WUC (Eq. 1) [18], SP (Eq. 2) [34], and change in size (Eq. 3) [6] of the membranes were settled through the below Eq.

$$WUC\,(\%) = \frac{W_w - W_d}{W_d} x100 \tag{1}$$

$$SP\,(\%) = \frac{T_w - T_d}{T_d} x100 \tag{2}$$

$$Change\ in\ size\,(\%) = \frac{A_w - A_d}{A_d} x100 \tag{3}$$

Herein, the symbols W, T, and A represent the weight, thickness, and area of the membrane, respectively. In addition, w used as a subscript represents the wet membrane, while d represents the dry membrane.

IEC is one of the fundamental experiments for assessing the proton conductivity of the membrane. In the IEC experiment, the membranes were subjected to a 24-h drying process at 100°C. Subsequently, the protonation procedure was employed on these membranes. During the protonation process, the membranes were plunged into sulfuric acid for a day and, after a day, in pure water [40, 63]. The purpose of the protonation process is to activate the membrane and increase the activation of ion exchange groups. Following the protonation, the membranes were delved into roughly equal-sized pieces and weights and placed in a 0.1 M NaCl solution for 48 h. After these 48 h, the membranes were extracted from the NaCl solution and titrated using a 0.01 M NaOH solution. These titrations were carried out using the Shott TA500 plus brand and model, a computer-controlled titration device with a precision of 0.01 mL. The titrant consumed at pH seven was recorded, and the IEC values of the membranes were computed utilizing Eq. 4 [64].

$$IEC = \frac{V_{NaOH} \times M_{w,NaOH}}{W_d} \tag{4}$$

Here, V_{NaOH} represents the amount of titrant NaOH spent in mL and $M_{w,NaOH}$ represents the molecular weight of NaOH used as titrant.

The mechanical strength, a critical factor in determining their lifespan within a fuel cell, was assessed using DMA. DMA was conducted using a Shimadzu mechanical analyzer. To prepare all samples for analysis, they were soaked in DI water for a day. Then, tensile strength tests were conducted at room temperature with a tensile speed of 3 $mm.min^{-1}$. Since the membranes are in constant contact with water in the fuel cell, their hydrolytic stability is vital to membrane longevity. To assess this, hydrolytic stability experiments were conducted on the synthesized membranes. Prior to the test, the membranes were dried in an oven at 100°C for one day and weighed. Subsequently, they were placed in deionized water at 80°C, the operating temperature of the PEMFC, for a specified duration. Before taking measurements, the membranes were removed from the water, dried at 100°C to eliminate moisture, and re-weighed. This process was repeated multiple times to determine the hydrolytic stability of the synthesized membranes. A crucial parameter for safeguarding the membrane structure against potential hydroxyl radicals that may arise within the fuel cell is oxidative stability. This was determined using a Fenton test (3% hydrogen peroxide by weight (H_2O_2, Sigma-Aldrich, 30%) and 4 ppm Fe^{2+}). Like the hydrolytic stability test, membrane pieces of appropriate sizes were dried at 100°C and weighed. They were then immersed in a Fenton solution at 80°C and room temperature. The samples were removed from the Fenton solution at specific intervals, dried at 100 °C, and re-weighed. This process was repeated multiple times to determine the oxidative stability of membranes. Impedance analyses were employed to determine the proton conductivities of the membranes. Proton conductivities of the synthesized membranes were measured using the four-probe technique. These measurements were conducted using a CH680 potentiostat device (30 to 80°C at 100% relative humidity). Prior to the measurements, the protonation process was applied to membranes. The membrane was placed in a BT-112-coded conductivity cell, and measurements were taken. The proton conductivity of the membrane was calculated using Eq. 5 [48] based on the membrane resistance measured from the Nyquist diagram.

$$Proton\ Conductivity = \frac{L}{R \times W_{th} \times T_d} \quad (5)$$

Herein, L is the distance between the electrodes, R is the membrane resistance, and W_{th} is the membrane width.

Membrane Electrode Assembly (MEA) Manufacturing and Single-Cell Performance Test

A membrane electrode assembly (MEA) was elaborated using the synthesised membrane prior to the PEMFC single-cell performance test. Before MEA was constructed, the membrane underwent protonation, following the same method previously employed for IEC measurement and impedance analysis. In the MEA, a gas diffusion layer made of 40% platinum-loaded carbon paper with a loading of 0.3 mg/cm^2, sourced from the Fuel Cell Store, was utilized. After the protonation process, 5% Nafion solution, as an ionomer, was applied to the membrane surface to ensure complete adhesion and placed between two carbon papers cut to 5 cm^2. The membrane assembly placed between carbon paper was subjected to hot pressing at 120°C under 1000 kgf pressure for 3 min, and thus MEA was prepared.

The FC performance tests of the membranes were conducted using a Fideris brand test station. Adjacent to the test station, a humidification unit was employed to ensure precise fuel cell conditions. Before the performance measurements, the prepared MEA was inserted into an Electrochem branded EFC-05-02 model single-cell fuel cell (serpentine-type flow channels, 5 cm^2 area). Then, nitrogen gas was passed through the humidification unit maintained at 70°C to humidify it to a 100% relative humidity and then fed to the cell for 3–4 h to active the membrane in the cell and provide proton conduction. For performance measurements, hydrogen/dry air was fed at 100% relative humidity in a stoichiometric (1/2) ratio, and the FC temperature was brought to 80°C. As a result of the conditioning process, membranes' current and power densities were obtained.

Results and Discussions

FTIR Analysis

FTIR analyses were conducted to assess the structural properties of the synthesized membranes and to ascertain the success of the synthesis of FBA-additive blend membranes. The spectra acquired from FTIR analyses performed on FBA-additive SPEEK-PVA blend membranes with varying weight ratios are presented for comparison in Fig. 3.

In the spectrum of FBA, three distinctive peaks were identified, with their centers at 1011, 1630, and 3540 cm^{-1}. It was established that the primary peak at 1011 cm^{-1} corresponds to FBA and is associated with the vibration of BF_4 stress [65, 66]. The peak at 3540 cm^{-1} is attributed to the stretching vibration of OH (hydroxyl) groups, while the peak at 1630 cm^{-1} corresponds to the bending vibrations of H-O-H molecules [67, 68]. The prominent peaks observed at wavenumbers 1255 cm^{-1}, 1080 cm^{-1}, and 1020 cm^{-1} in the FTIR spectrum of all the membranes are indicative of symmetric and asymmetric O = S = O stretching vibrations. These peaks strongly suggest the presence of sulfonic acid groups in the membranes [6, 40, 69, 70]. Furthermore, the peak at the wavenumber 2910 cm^{-1}, representing the asymmetric stretching of C-H bonds in CH_2 species, suggests the presence of PVA in the membrane's structure [40, 71]. The characteristic peaks of SPEEK and PVA overlap with the distinctive peaks of FBA, making it difficult to distinguish them from one another in the FTIR spectra. Nevertheless, in the FTIR patterns of the membranes, it was observed that the peak intensities centered at 1011 cm^{-1}, 1630 cm^{-1}, and 3540 cm^{-1} increased as the FBA additive ratio was raised. This outcome from the FTIR analyses suggests successfully integrating the FBA additive material into the membrane matrix.

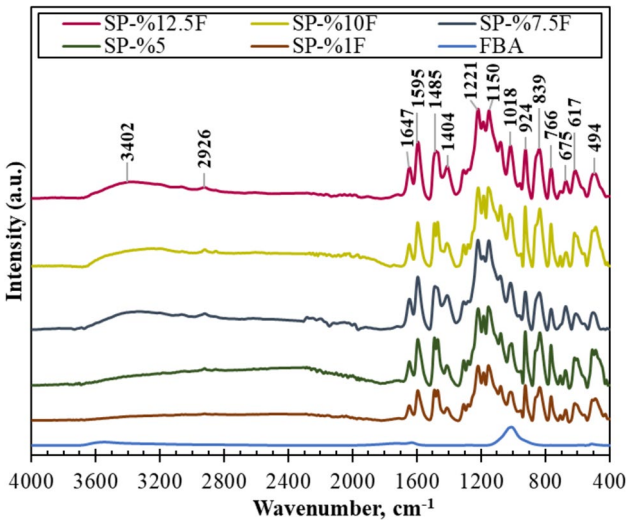

Fig. 3 FTIR spectra of FBA-additive blend membranes

XRD Analysis

The impact of the crystallinity of the membranes employed in PEMFC on proton conductivity is well-recognized. Consequently, XRD analyses were conducted to ascertain the crystalline phase, crystallinity, and degree of crystallinity in the blend membranes. XRD patterns of FBA-additive blend membranes with different weight ratios are comparatively given in Fig. 4.

In the XRD patterns of the membranes, four peaks centered approximately at 2Θ = 18.95°, 23°, 29°, and 38.7° were

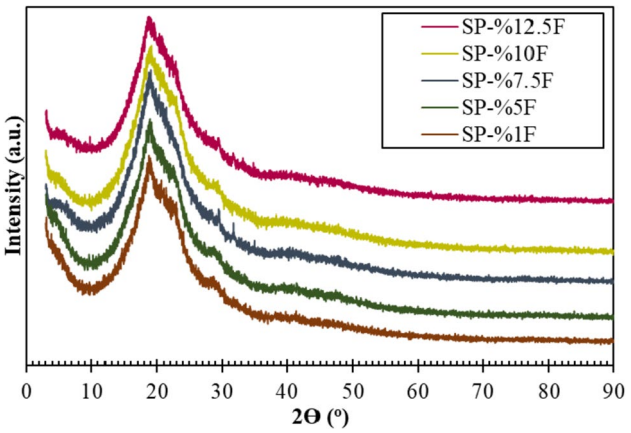

Fig. 4 XRD patterns of FBA-additive blend membranes

Table 2 Crystallinity and average crystal size of the synthesized membranes

Membrane	Crystallinity (%)	Average crystal size (nm)
SP-%1 F	64.46	2.51 ± 1.72
SP-%5 F	66.71	2.53 ± 1.81
SP-%7.5 F	69.86	2.56 ± 1.83
SP-%10 F	66.93	2.20 ± 1.01
SP-%12.5 F	60.88	2.44 ± 1.79

observed in the XRD pattern. The semi-crystalline structure of PVA has two prominent characteristic peaks at 19.5° and 38.6° [72–74]. This PVA structure has been attributed to intramolecular and intermolecular hydrogen bonds. These hydrogen bonds can form between molecules within a single monomer unit or between molecules in different monomer units, contributing to the observed semi-crystalline nature of PVA [72]. In addition, 2Θ = 20–30° for the 110, 111, 200, and 211 planes of the semi-crystalline PEEK polymer, and as a result of sulfonation, a broad peak is formed in SPEEK due to the bonding of SO_3H groups to PEEK in the 110 plane around 2Θ = 22° [75, 76]. Also, the peak at 2Θ = 38° belongs to SPEEK [77, 78]. Because FBA lacks a crystalline structure, it doesn't manifest as peaks in the XRD patterns. However, it is believed to influence the crystallinity and the average crystal size of the membranes. Deconvolution analysis was conducted to gain a more precise understanding of the crystallinity and average crystal size of the membranes. The crystallinity values, average crystal sizes of the membranes, and the graphical results obtained from the deconvolution process are presented in Table 2; Fig. 5, respectively.

The crystallinity and average crystal size of FBA-additive membranes increase steadily with the increasing FBA content of the membrane up to 7.5 wt% FBA additive. Further increase in FBA causes decrease in crystallinity and average crystal size of the membrane. Six effects can increase the crystallinity of polymers. These are a regular and symmetrical linear chain, low degree of polymerization, intermolecular solid forces, small and regular pendant groups, slow cooling rate, and oriented molecules [79, 80]. It is thought that FBA added to the membrane matrix, up to a certain weight%, forms strong intermolecular forces with SPEEK and PVA, increasing the degree of crystallinity of a regular and symmetrical linear chain. Narrow molecular weight, linear polymer chains, and a higher molecular weight enhanced the membrane's crystallinity. Moreover, the XRD patterns show a noticeable shift of crystal peaks toward higher angles as the weight% of FBA in the membrane matrix increases. This shift towards higher Bragg angles signifies the establishment of robust bonds within the membrane matrix [81]. In the literature, studies indicate that crystallinity will positively affect the membrane performance [82–85], as well as studies showing that the performance will decrease with increasing crystallinity [86–88]. In the structure of the synthesized membranes, it is thought that the coexistence of amorphous and crystalline structure and the fluorine bonds from FBA, which are expected to have a positive effect on proton conductivity, are the main reason for increasing crystallinity and will have a positive impact on fuel cell performance. In an ordered molecular structure, protons will be transferred faster than in a disordered structure, and an Arrhenius-type proton conduction mechanism will contribute positively to the performance due to the increase in the glass transition temperature with increasing crystallinity. Similar to the crystallinites, it was determined that the average crystal size increased up to 7.5% FBA by weight and then decreased. As a result of XRD studies, it is understood from the varying degree of crystallinity and average crystal sizes that FBA was succesfully added into the SPEEK-PVA matrix at different percentages. When the average crystal sizes and degrees of crystallinity of the membranes are evaluated together, it is thought that the decrease in membrane crystallinity at ratios above 7.5% FBA by weight is due to the formation of agglomeration. SEM analyses were performed with FBA-additive membranes to understand this situation more clearly.

SEM Analysis

SEM analysis was performed to investigate alterations taking place on the membrane's surface as a result of the introduction of FBA and to characterize their structure. Figure 6 presents SEM images of the membranes.

In membranes containing 5% and 7.5% FBA by weight, it is observed that FBA is homogeneously and uniformly distributed in the membrane matrix. At higher ratios, it was noticed that agglomeration and channels were formed on the

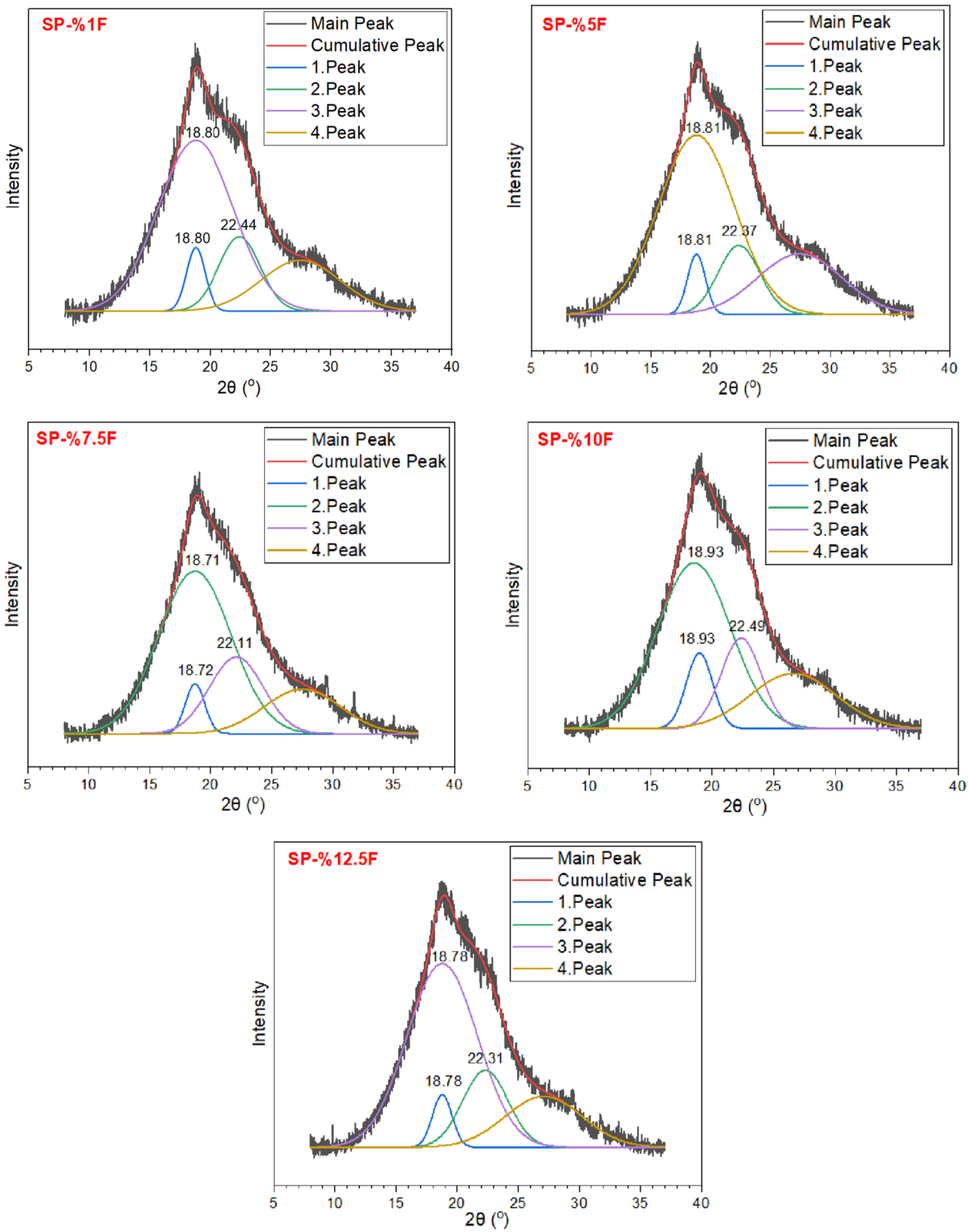

Fig. 5 Deconvolution implemented to XRD patterns of membranes

membrane surfaces. The large particles formed indicate that the FBA additive is collected in certain places, and there is no homogeneous distribution. Following a specific additive content (7.5% by weight), FBA, which couldn't penetrate the membrane matrix, was instead deposited on the surface of the membrane matrix. The findings related to crystallinity

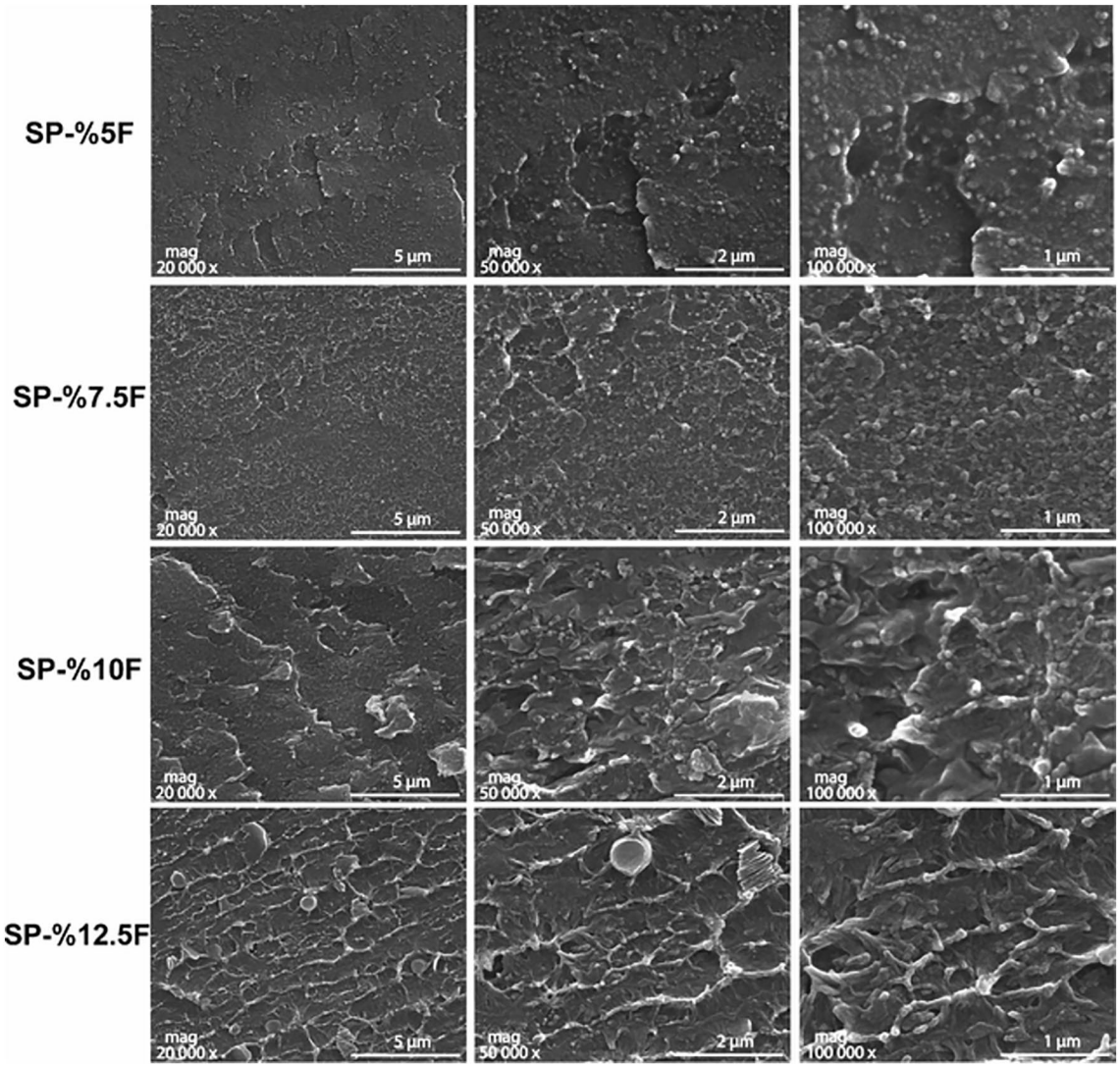

Fig. 6 SEM images of the cross-sectional area of FBA-additive membranes

and average crystal size also corroborate this observation. The agglomeration process led to a reduction in both the crystallinity and average crystal size of the membrane. Furthermore, as evident from the SEM images, a non-porous structure was achieved in all fabricated membranes, as intended.

TGA-DTG and DSC Analyze

TGA-DTG analyses were conducted to assess the thermal stability of the membranes containing FBA additives, and DSC analyses were executed to ascertain the glass transition temperatures (Tg). Figure 7 displays the comparative TGA and DTG thermograms of the membranes.

The synthesized membranes retained over 60% of their total weight up to a temperature of 600 °C. It was further observed that the weight loss diminished with an increased proportion of the additive material within the membrane structure. This phenomenon can be attributed to the interfacial interaction among SPEEK, PVA, and FBA. In addition, another reason for the increased thermal stability with the addition of FBA is due to the thermal resistance-enhancing properties of boron and fluorine [89]. It was determined that all membranes had the same degradation steps at almost the same temperatures. It is seen that a 3-step degradation occurs for each membrane. The first weight loss occurred between 80-210 °C, and the degradation between these temperatures is due to physically absorbed water or humidity [90, 91]. In the second weight loss between 245-440 °C, both the desulfonation of the $-SO_3H$ groups takes place in the side chain of PVA and some of in the main chain are degraded [92, 93]. The last and most significant weight loss was determined due to the degradation of the main chain of SPEEK and PVA polymers [94, 95]. In addition, the degradation

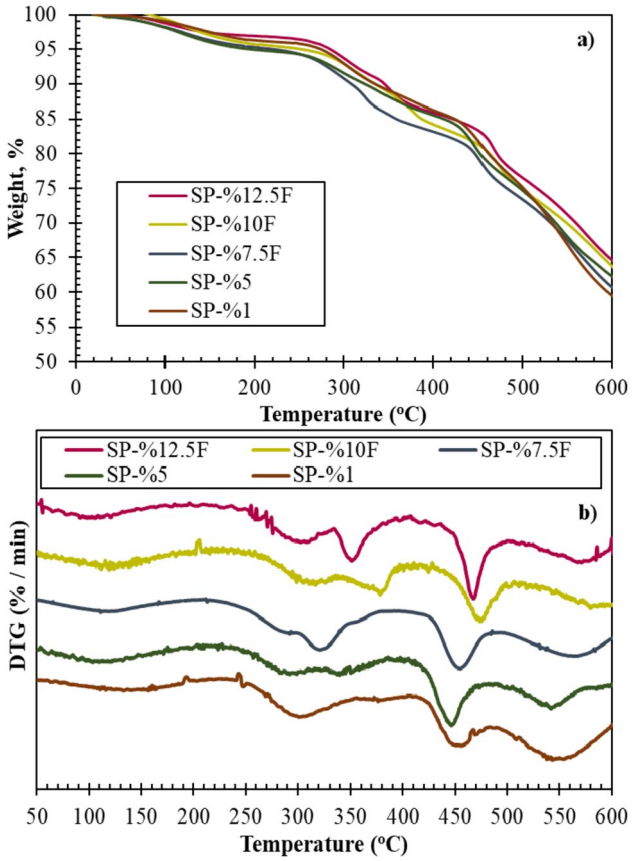

Fig. 7 **a** TGA thermograms, **b** DTA thermograms of FBA-additive membranes

temperature of HBF_4 groups is between 160–500 °C, and the weight loss between these temperatures is related to FBA [96]. The synergy of FBA with SPEEK and PVA is thought to enable the sulfonic acid groups and the main chain of PVA to degrade more slowly with increasing temperature and increased thermal strength. This is supported by the shape of the exothermic peak between 400-450 °C in the DTG thermogram. In this temperature range, a single peak was observed in the membranes. The single peak shows the degradation of a single structure due to synergy with the FBA entering the structure.

DSC analyses were conducted to investigate changes in the T_g of the membranes about the FBA ratio. The first-order derivative of heat flux was utilized to enhance the clarity of T_g determination. Figure 8 presents the DSC thermograms of the membranes. T_g, an indicator of the membrane's thermal resistance, reflects its capacity to withstand temperature and humidity conditions within the fuel cell environment. Additionally, T_g is one of the parameters that influences the ionic conductivity of the membrane. If the operational temperature of the fuel cell is lower than the glass transition temperature of the membrane, proton conduction follows the Arrhenius law. Conversely, if the temperature exceeds T_g, Vogel-Tammen-Fulcher (VTF) law governs proton conduction [22]. It was determined that T_g increased up to 7.5% FBA additive and decreased at higher ratios. T_g increases with the crystallinity of the membranes [97, 98]. As a result of the increase in the crystallinity of the structure, segmental movement in the membrane matrix is restricted. The limitation of bond mobility within the membrane structure resulted in an elevation of the T_g of the membranes. The fact that the T_g of FBA-additive membranes surpasses the operating temperature of the PEMFC is believed to have a beneficial impact on proton conductivity. Furthermore, the higher T_g of the membranes offers the opportunity for operation at elevated temperatures.

Water Uptake Capacity (WUC), Swelling Properties (SP) and Change in Size

The performance of membranes utilized in fuel cells is significantly influenced by three crucial parameters: WUC, SP, and change in size. While a high WUC is desirable in membranes, low values for SP and dimensional changes are preferred. With an increase in humidity within the membrane structure, resistance decreases, and proton conductivity improves, as proton conduction relies on the presence of water molecules. However, as swelling and thickness increase, mass transfer resistances gradually rise, decreasing proton conductivity. Additionally, size changes can lead to membrane deformation and tears. The outcomes of WUC, SP, and change in size measurements performed on membranes at room temperature and 80 °C are depicted in Fig. 9.

The WUCs of the membranes increased steadily at both room temperature and 80°C up to 7.5% FBA additive. Among the synthesized membranes, the highest WUC values were obtained, with the membrane containing 7.5% FBA by weight with 15.62% at room temperature and 16.44% at 80°C. It is seen that the WUCs of the synthesized membranes are lower compared to Nafion. It is thought that FBA additive and thermal crosslinked reduce the WUC of the membrane. There may be two reasons for the decrease in the WUC of membranes due to FBA additive. Firstly, fluorine in the FBA structure is hydrophobic, reducing the WUC [99, 100]. Secondly, stronger bonds were formed due to thermal crosslinking with inorganic additives, and membrane density increased. This resulted in a decrease in the molecular gap. The crystallinity also confirms this situation. A material's crystallinity significantly affects WUC, and uniformly structured crystalline materials tend to have higher WUC than amorphous materials [101–103]. However, an increase in WUC was observed with an increase in the amount of FBA up to 7.5% by weight. This situation shows that the hygroscopic property of boron is emphasized with the FBA additive. At 80°C, WUC values increased slightly with ionic mobility.

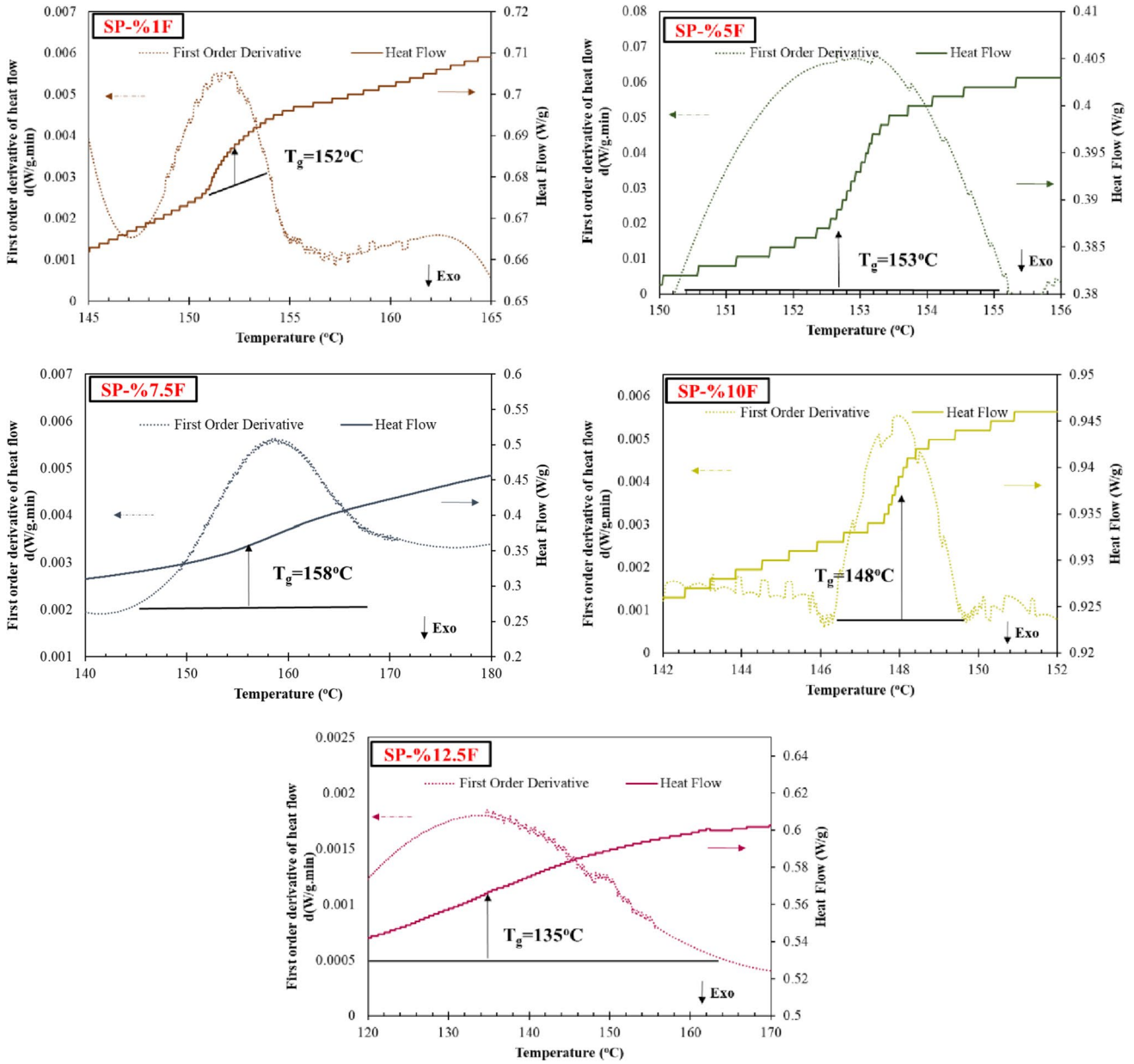

Fig. 8 DSC thermograms of FBA-additive blend membranes

Under normal conditions, these values are expected to increase more, but the shortened bonds after thermal crosslinking and the decrease in the molecular gap caused a more minor increase. It was determined that the reduction of the additive content higher than 7.5% FBA was due to agglomeration in the structure. As seen in the SEM images (Fig. 6), the high content of the additive material reduced the molecular gap to an undesirable extent. In addition, it is seen from the SP and change in size results that the molecular gap decreases due to the increase in the additive ratio. While the change in size of the membrane containing 1% FBA by weight is 14.68% at room temperature, this ratio is only 0.21% in the membrane containing 12.5% FBA. In addition, considering the change in thickness and change in size of the membrane with 12.5% FBA by weight, it can be seen that the standard deviation values are quite high. The thickness and size changes in different membrane parts differed due to accumulation, which caused the standard deviations to be increased. This situation is a result of agglomeration, as determined in SEM images, and this is also reflected in the change in thickness and change in size results. It is seen that the SP and change in size of FBA-additive membranes are pretty small compared to commercial Nafion-117. This shows

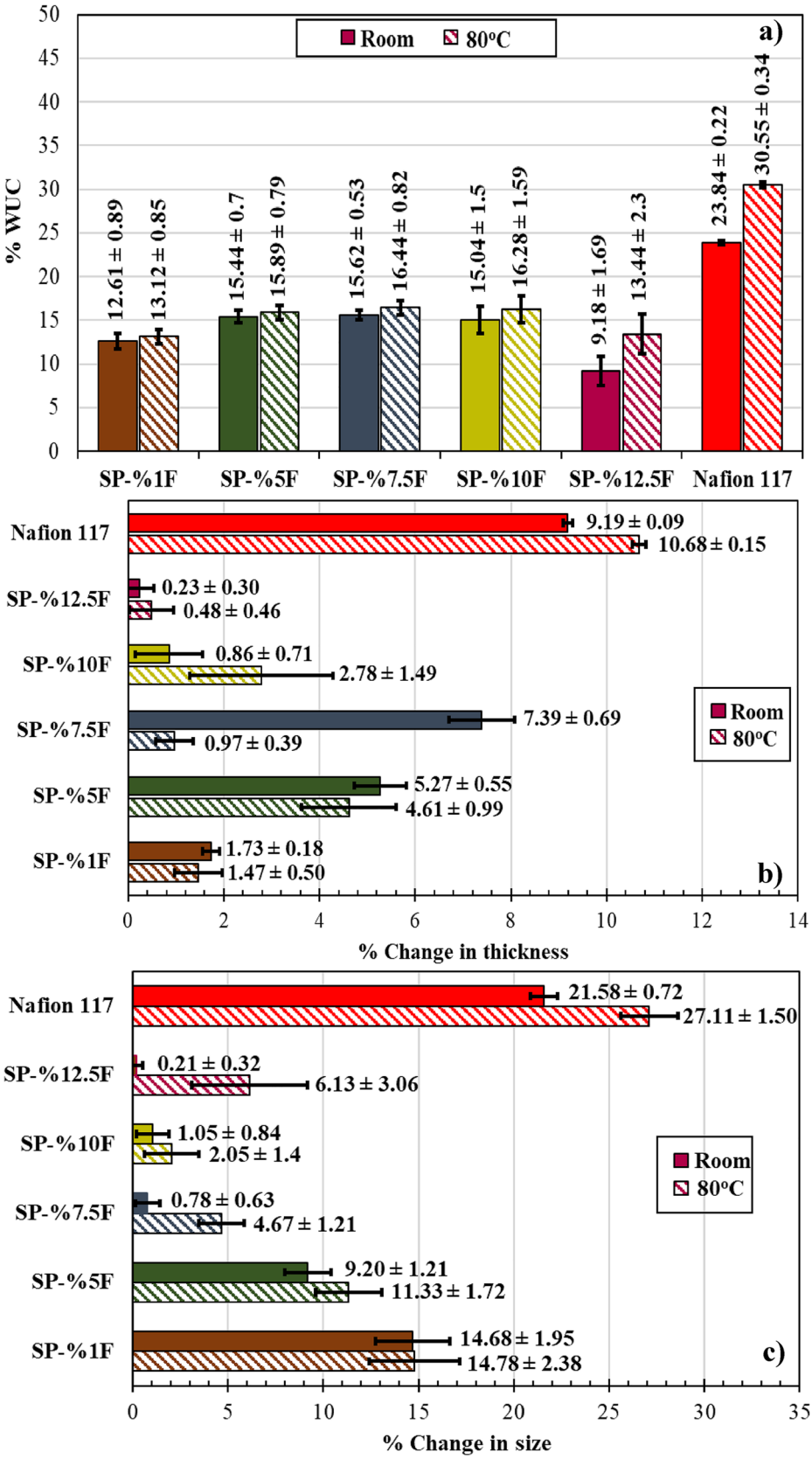

Fig. 9 **a** WUC, **b** SP, **c** change in size of FBA-additive blend membranes

that FBA-additive membranes will be much less affected by mass transfer resistances that may occur in the fuel cell.

Dynamic Mechanical Analysis

Dynamic mechanical analyses were conducted to evaluate the mechanical strength of FBA-additive membranes. The maximum tensile strength, young modulus, and elongation at break values obtained as a result of DMA are given in Table 3.

The mechanical strength results of the membranes are more or less similar. While average values were obtained for maximum tensile strength and Young's modulus values, elongation at break values was low. Subianto et al. obtained 34 MPa maximum tensile strength and 200% elongation at break value due to mechanical analyses performed with commercial Nafion membrane [104]. In the studies by different study groups, the maximum tensile strength ranged between 43 and 17.2 MPa. In contrast, elongation at break values ranged between 90% and 253% in the studies carried out with commercial membranes (Aquivion, Gore-Select, etc.) [104–106]. In physical observations, it was determined that the elongation values of the synthesised membranes were low and had a more brittle structure compared to commercial Nafion. The low values of the elongation at break of the membrane with the additive are due to the high crosslinking density, which prevents plastic deformation of the membrane [107]. Since more intense crosslinking occurs with adding FBA to the structure, the bonds in the membrane structure are shorter and lose their elasticity.

Table 3 Mechanical analysis results of FBA-additive membranes

	Maximum Tensile Strenght (MPa)	Young Modulus (MPa)	Elongation at Break (%)
SP-%1 F	21	175	9.8
SP-%5 F	44	263	12.4
SP-%7.5 F	44	262	12.8
SP-%10 F	42	261	13.8
SP-%12.5 F	40	258	12.1

Ion Exchange Capacity (IEC)

Tests were carried out to determine the IEC, which is a measure of the proton conductivity of the membranes, and the results obtained are given in Fig. 10. IEC values of FBA-additive membranes were found to vary between 1.55 and 0.94 meq/g. The highest IEC value was obtained as 1.55 meq/g with 7.5% FBA-additive membrane. IEC values were in parallel with the WUC of the membranes. This is thought to be due to the narrowing of intermolecular bonds after thermal crosslinking with the additive material and decreased proton conduction channels due to lower molecular spacing. In other words, access to the active sites in the membrane matrix is restricted due to reduced elasticity and increased stiffness due to thermal crosslinking. In addition to this situation, it was observed that the IEC values of the membranes increased due to the amount of FBA of up to 7.5% FBA content by weight. The main reason is the increased presence of fluorine, which has high electronegativity, in the membrane structure [108]. It was observed that IEC values decreased at higher FBA content. This result was in parallel with the results of many studies such as WUC, T_g, mechanical strength and it was concluded that it was a result of agglomeration in the structure.

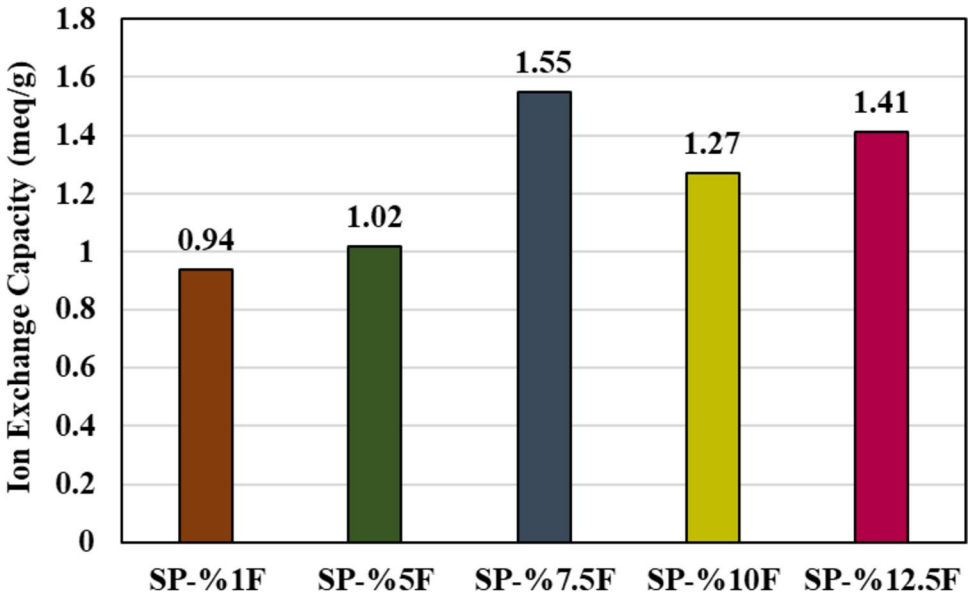

Fig. 10 IEC values of FBA-additive membranes

AC Impedance Analysis

AC impedance analyses were performed to determine the proton conductivity of FBA-additive membranes. Impedance analyses were performed at six different temperatures (30 °C, 40 °C, 50 °C, 60 °C, 70 °C, 80 °C), and the membranes' proton conductivity is comparatively given in Fig. 11. In addition, the activation energies of the membranes were calculated with the conductivity values obtained as a result of proton conductivity, and the mechanism effective in proton conduction was determined. Nyquist and Bode diagrams obtained with membranes synthesized as a result of AC impedance analysis are given in "Supplementary Information" section as Figure S1, S2, S3, S4, and S5.

In the previous study carried out by our research group, the highest proton conductivity value was reached as 0.195 S/cm at 80 °C with the SP blend membrane without FBA additive. Even with a 1% FBA additive, the proton conductivity of the membrane reached 0.258 S/cm and increased by approximately 32%. Introducing FBA into the membranes led to a noticeable increase in proton conductivity. The highest proton conductivity value reached an impressive 0.57 S/cm with a membrane additive with 7.5% FBA at 80 °C. These values significantly surpass the reference proton conductivity of commercial Nafion membrane, which stands

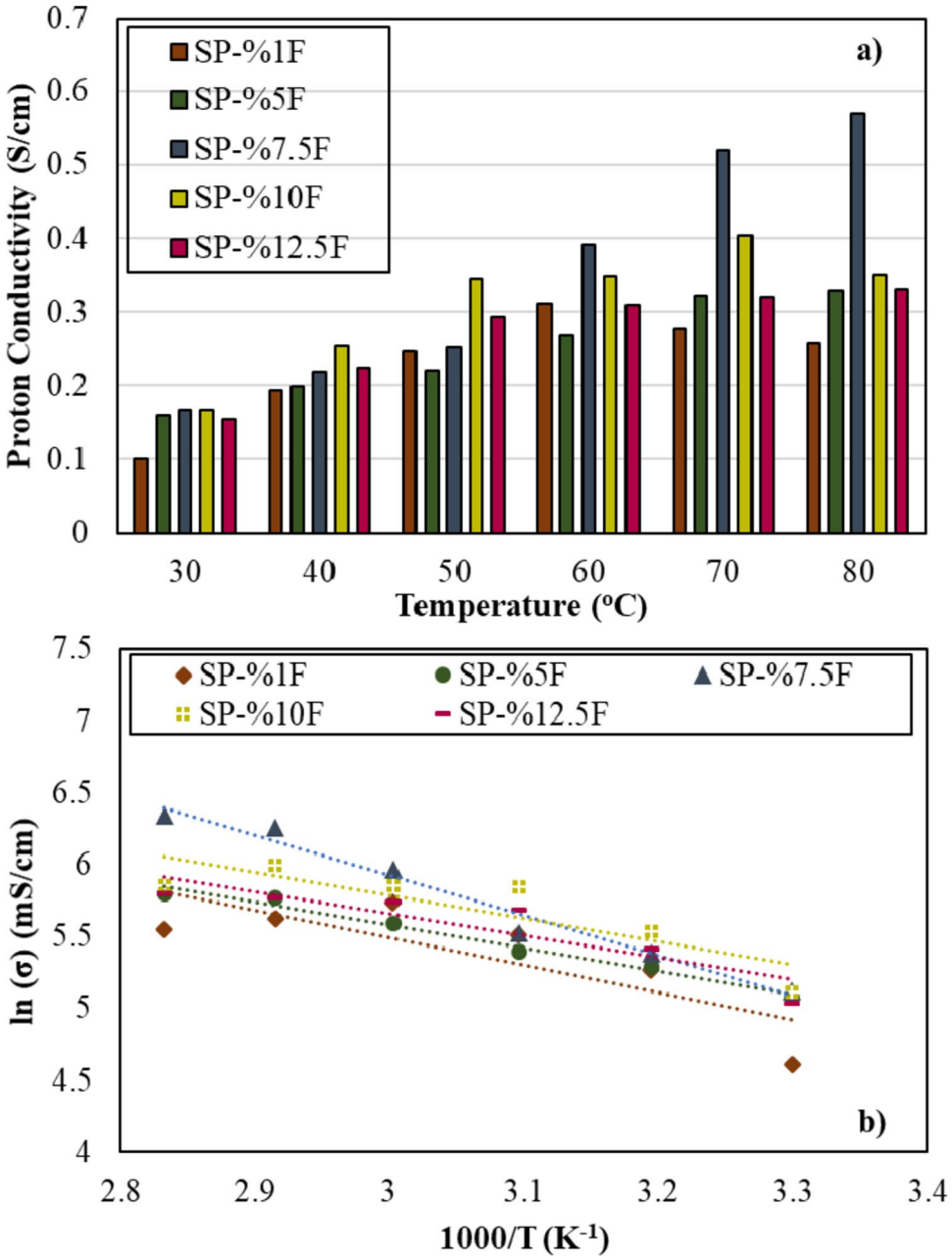

Fig. 11 **a** proton conductivities, **b** activation energies of FBA-additive membranes

at 0.1 S/cm at 30 °C. When compared to proton conductivity values reported in the literature, it is evident that the achieved proton conductivity values are notably high. For instance, Murmu et al. reported a proton conductivity of 0.07 S/cm at 80 °C with SPEEK-PVA-silica, Sahin et al. achieved 0.09 S/cm at 80 °C with SPEEK-PVA-TEOS, and Reyes et al. measured 0.083 S/cm at 130 °C with SPEEK-PVA-GO [18, 109, 110]. The primary rationale for selecting FBA as an additive material is to enhance proton conductivity. Fluorine plays a crucial role in promoting proton conduction by activating H^+ ions within the hydrogen bonds present in the structure. Moreover, the difference in electronegativities between boron (B) and fluorine (F) in the FBA structure influences the electron density around the B-F bonds, contributing to increased pore size [111]. Another reason for the increase in proton conductivity lies in the understanding that a decrease in proton conductivity in additive membranes at elevated temperatures is likely attributable to their low WUC and the hydrophobic nature of fluorine. Proton conduction primarily relies on the presence of water molecules, and as water evaporates at higher temperatures, proton conductivity diminishes. Furthermore, a decline in proton conductivity was observed in membranes with additive ratios exceeding 7.5% FBA by weight, a phenomenon consistent with prior analyses. The reduction in crystallinity, diminished WUC, and the formation of agglomerates contribute to the decrease in proton conductivity within the membranes. The closure of active sites due to a reduction in free volume within the membrane matrix is believed to be the primary cause behind the decline in proton conductivity, even as the FBA ratio increases. Notably, the activation energies of FBA-additive membranes ranged from 13.35 kJ/mol to 23.28 kJ/mol, indicating that proton conduction occurs via the Grotthuss mechanism.

Hydrolytic Stability

Hydrolytic stability is one of the essential properties sought in membranes to be used in PEMFC and is the primary obstacle for the structure to be used as an electrolyte membrane in a fuel cell [112]. Long-term hydrolytic stability tests with the synthesized additive membranes were carried out at 80 °C, the operating temperature of PEMFC. The hydrolytic stability test results of the membranes are given in Fig. 12. As a result of the 900 h hydrolytic stability test, FBA-additive membranes maintained their weight between 78 and 80%. Based on these results, it can be said that the membranes have very high stability. In addition, it was determined that the FBA additive positively affected the hydrolytic stability of the membrane. It is thought that the primary reason for such high hydrolytic stability in all membranes is thermal crosslinking and then FBA

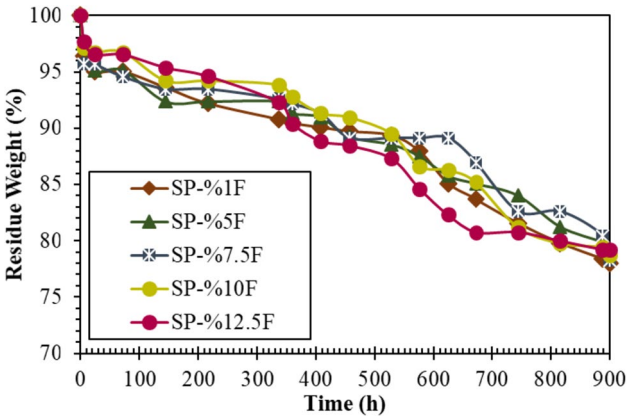

Fig. 12 Hydrolytic stability of FBA-additive membranes at 80 °C (900 h)

additive. The studies in the literature show that the thermal crosslinking process increases hydrolytic stability [113, 114]. Highly polar water molecules have been reported to weaken the electrostatic interactions (Van der Waals) between SPEEK molecular chains and decrease durability [115]. On the other hand, it has been reported that the presence of OH groups with the high hydrophilic character of PVA has a negative effect on hydrolytic stability [18]. However, thermal crosslinking increases the densities of the membranes and limits the polymer chain movement inside the membranes, thus increasing the hydrolytic stability [113]. The decrease in the presence of −OH and $-SO_3H$ groups in the structure due to the reaction of −OH and $-SO_3H$ groups with the thermal crosslinked reaction strengthens hydrolytic stability. In addition, it is concluded that the structure is tighter due to thermal crosslinking with the additive material, and the membrane structure becomes more stable due to closing the open ends with strong bonds. This is in parallel with the crystallinity, and XRD results prove that the chain movement is limited. Considering the hydrolytic stability results in the literature, Soosan et al. observed the first weight loss of the membrane at the end of the 10th hour in the hydrolytic stability experiment carried out at 60 °C temperature with the SPEEK membrane they synthesized. They stated that the membrane lost approximately 23% of its total weight at the end of the 60th hour [115]. Akbarian-Feizi et al. performed hydrolytic stability tests of the membranes they synthesized at 80 °C and reported that membranes with different weight DABS-DAH ratios maintained hydrolytic stability for 3 h, 7 h, and more than 100 h [116]. Tamura and Kawakami, in their study on composite and nanofibre membranes, reported that the composite membrane was wholly dissolved after 1400 h at 80 °C, and the nanofibre membrane was dissolved entirely after 1600 h [117].

Table 4 Oxidative stability of FBA-additive membranes

Membrane	Residue weight (1 h)	Residue weight (3 h)	Physical status
SP-%1 F	%94.94	%89.45	Brittle
SP-%5 F	%93.65	%84.24	Brittle
SP-%7.5 F	%93.83	%90.82	Brittle
SP-%10 F	%79.95	%59.21	Ruptured
SP-%12.5 F	%87.63	%76.36	Ruptured

Oxidative Stability

Apart from hydrolytic stability, another factor determining the service life of membranes is their oxidative stability. The Fenton test determined the oxidative resistance of FBA-additive membranes, and the oxidative stability of membranes are given in Table 4.

During fuel cell operation, the formation of hydroxy and peroxy radical groups is a concern, as these reactive species can potentially attack the membrane matrix and lead to membrane degradation. This degradation can negatively impact the performance and lifespan of the fuel cell. Mitigating such degradation and enhancing membrane durability is essential [114]. In the literature, the oxidative stability of membranes developed for PEMFC applications was generally carried out at room temperature or 60 °C [18, 118, 119]. The Fenton test, conducted at the operating temperature of the fuel cell (80 °C), aimed to replicate natural conditions. It revealed a reduction in the membranes' oxidative stability upon adding FBA. FBA, being a potent acid, substantially heightened the acidity of the membrane. This increased acidity made the proton exchange sites more reactive. Consequently, the enhanced reactivity of these sites increased the likelihood of free radicals in the environment reacting with them, leading to accelerated degradation and decreased oxidative stability of the membranes. Notably, the pronounced decline in the oxidative stability of membranes additives with 10% and 12.5% FBA by weight can be attributed to structural aggregation and reduced mechanical strength.

Fuel Cell Performance Test

A single-cell fuel cell performance test was carried out with an SP-%7.5 F coded membrane, which gave the best results in the characterization studies. In addition, a performance test was carried out with Nafion-117 purchased from Ion-Power, and the comparative result is given in Fig. 13.

The prepared MEA was placed in the fuel cell, and to prevent high deviations in potential and current density changes, a 20-h conditioning procedure, determined from our research group's previous experiences at the fuel cell test station, was applied. The conditioning process was started

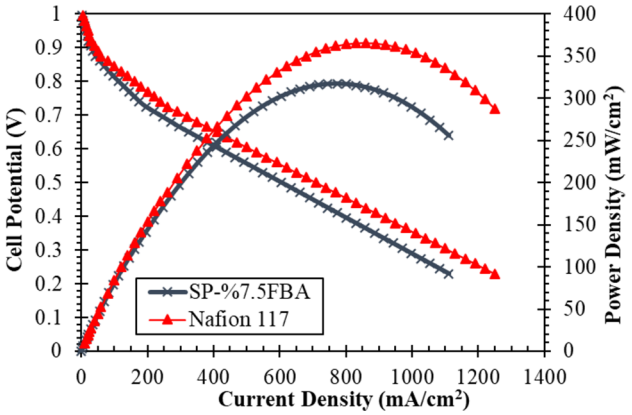

Fig. 13 Single-cell performance test results of SP-%7.5 F and Nafion-117

by applying 0.6 V, 0.8 V, 1 V, 0.8 V, 0.6 V, 0.4 V, and 0.2 V, respectively, each lasting 2 h. Following this 14-h process, the MEA was exposed to 0.6 V for 6 h, and the 20-h conditioning process was completed. The performance tests revealed that the commercial Nafion-117 membrane exhibited slightly higher current and power densities than the SP-%7.5 F coded membrane. Specifically, at a cell potential of 0.6 V, Nafion-117 achieved a current density of 510 mA/cm^2 and a power density of 306 mW/cm^2. At the same time, SP-%7.5 F attained a current density of 418 mA/cm^2 and a power density of 250.8 mW/cm^2. The performance results of commercial Nafion-117 were much better than impedance analyses, and higher current density and power density were obtained from the synthesized membrane. In the AC impedance results of the membrane coded SP-7.5 F, higher proton conductivity is obtained than Nafion 117, and it has been observed that this situation is the opposite in fuel cell performance. Impedance analysis measures the proton conductivity of the membrane resulting only from membrane resistance. The effect of other parameters that make up the membrane's fuel cell performance does not affect this analysis. Indeed, a fuel cell's performance is influenced by many factors, and the properties of the membrane play a crucial role in determining the overall cell performance. Factors such as the WUC of membranes, the presence of active groups in the polymer chain, hydrolytic resistance, and mechanical strength directly impact the cell performance of the membrane [18]. The commercial membrane has a higher WUC, hydration degree, and more stable structure compared to the synthesized membranes, enabling higher values in performance tests. In the previous study of our study group, a current density of 262 mA/cm^2 and a power density of 158.51 mW/cm^2 was obtained at a cell potential of 0.6 V with a SPEEK-PVA blend membrane [40]. It is seen that the membrane performance increases considerably with the FBA additive. Especially fluorine, which is present in the

FBA structure and has high electronegativity, is thought to have the highest contribution to this performance increase. It is considered that the reduction of sulfonic acid groups and molecular void volume in the structure due to thermal crosslinked causes the synthesized membrane to perform less than its potential.

Conclusion

In this study, a novel fluoroboric acid-additives SPEEK-PVA blend membrane, which has not been used in PEMFC before and has a very high potential, was studied. To identify the most suitable FBA additive, a series of SPEEK-PVA blend membranes were prepared with varying FBA content, specifically 1%, 5%, 7.5%, 10%, and 12.5% by weight, followed by a comprehensive characterization study. The results of these studies confirmed the successful synthesis of the membranes, particularly as evidenced by XRD and FTIR analyses. Furthermore, it was observed that the crystallinity of the membranes increased with the FBA additive, a phenomenon attributed to the presence of strong intermolecular forces and the establishment of a regular and symmetrical linear chain within the membranes. These findings are indicative of the successful integration of FBA as an additive in the membrane composition. Additionally, it was noted that the crystallinity, T_g, and WUC of membranes containing FBA increased consistently up to a 7.5 wt% FBA additive but declined at higher concentrations due to aggregation, as indicated by SEM analyses. It was determined that the maximum tensile strengths of FBA-additive membranes were at average values, but the elongation at break values was quite low. This is due to the high crosslinking density which prevents plastic deformation of the membrane. The membranes exhibited relatively high IECs and proton conductivity chiefly due to the strong electronegativity of fluorine in the FBA structure. The membrane's highest proton conductivity was achieved with 7.5% FBA by weight, surpassing commercial Nafion-117. Hydrolytic stability improved with the FBA additive, and the decrease in the presence of -OH and $-SO_3H$ groups in the structure through thermal crosslinking reactions contributed to this enhancement. In oxidative stability tests, FBA-additive membranes were found to have a brittle structure. The main reason for this is that the rise in the acidity of the membrane with the addition of FBA, which is a strong acid, caused the proton exchange sites to become more reactive, and a faster degradation occurred as a result of the increased possibility of free radicals in the media to react with reactive sites. As a result of the characterization studies, the most suitable FBA additive ratio was 7.5% by weight, and a single-cell performance test was carried out with this membrane. As a result of the performance test, 418 mA/cm^2 current density and 250.8 mW/cm^2 power density were obtained with the SP-%7.5 F coded membrane. The results obtained, especially the effect of FBA on the proton conductivity of the membrane to very high levels and its impact on the performance, showed that it is a promising structure. Although the performance values obtained are slightly lower than commercial Nafion, synthesis of the SP-7.5%F coded membrane is approximately 63% more economical than Nafion. In addition, the high performance and low-cost exhibited by FBA-additive membranes will take its place among the membranes that can be an alternative to commercial membranes in the literature.

Supplementary Information The online version contains supplementary material available at https://doi.org/10.1007/s10924-023-03180-7.

Acknowledgements This research was endorsed by The Scientific and Technological Research Council of Turkey (TUBITAK 2211/A National PhD Scholarship Program) and Gazi University Scientific Research Fund (Project code: FYL-2022-8059 and project code: FGA-2022-7454).

Author Contributions Y.Y. carried out the synthesis studies. Y.Y. and I.A. carried out both characterization studies and performance test studies. Y.Y. and I.A. both evaluate the experimental experimental outcomes. The manuscript was written by Y.Y., and checked by I.A. Both authors reviewed the manuscript.

Funding Open access funding provided by the Scientific and Technological Research Council of Türkiye (TÜBİTAK).

Declarations

Competing Interests The authors declare no competing interests.

References

1. Koçyiğit Çapoğlu İ, Uysal D, Doğan ÖM (2023) Mass transfer studies for CO_2 absorption into carbitol acetate as an effective physical absorbent using a laboratory-scale packed column. Heat Mass Transf 60:133–145. https://doi.org/10.1007/s00231-023-03427-y
2. Haque M, Sulong A, Majlan E, Loh K, Husaini T, Rosli R (2019) Physiochemical characteristics of solid electrolyte membranes for high-temperature PEM fuel cell. Int J Electrochem Sci 14:371–386. https://doi.org/10.20964/2019.01.26
3. Öztan H, Çapoğlu İK, Uysal D, Doğan ÖM (2023) A parametric study to optimize the temperature of hazelnut and walnut shell

gasification for hydrogen and methane production. Bioresource Technol Rep 23:101581. https://doi.org/10.1016/j.biteb.2023.101581
4. Shen X, Liang X, Xu Y, Yu W, Li Q, Ge X, Wu L, Xu T (2023) In-situ growth of PPy/MnOx radical quenching layer for durability enhancement of proton exchange membrane in PEMFCs. J Membr Sci 675:121556. https://doi.org/10.1016/j.memsci.2023.121556
5. Zhao Y, Lv B, Song W, Hao J, Zhang J, Shao Z (2023) Influence of the PBI structure on PBI/CsH5(PO4)2 membrane performance for HT-PEMFC application. J Membr Sci 674:121531. https://doi.org/10.1016/j.memsci.2023.121531
6. Yagizatli Y, Ulas B, Sahin A, Ar I (2022) Investigation of sulfonation reaction kinetics and effect of sulfonation degree on membrane characteristics for PEMFC performance. Ionics 28:2323–2336. https://doi.org/10.1007/s11581-022-04494-7
7. Liu Q, Li X, Zhang S, Wang Z, Chen Y, Zhou S, Wang C, Wu K, Liu J, Mao Q (2022) Novel sulfonated N-heterocyclic poly (aryl ether ketone ketone) s with pendant phenyl groups for proton exchange membrane performing enhanced oxidative stability and excellent fuel cell properties. J Membr Sci 641:119926. https://doi.org/10.1016/j.memsci.2021.119926
8. Çelik Kazici H, Yildiz F, İzgi MS, Ulaş B, Kivrak H (2019) Novel activated carbon supported trimetallic PdCoAg nanoparticles as efficient catalysts for the hydrolytic dehydrogenation of ammonia borane. Int J Hydrog Energy 44:10561–10572. https://doi.org/10.1016/j.ijhydene.2019.02.198
9. Er OF, Caglar A, Ulas B, Kivrak H, Kivrak A (2020) Novel carbon nanotube supported Co@Ag@Pd formic acid electrooxidation catalysts prepared via sodium borohydride sequential reduction method. Mater Chem Phys 241:122422. https://doi.org/10.1016/j.matchemphys.2019.122422
10. Yörük Ö, Ziraman DU, Doğan ÖM, Uysal BZ (2019) Çan linyitinden elektroliz yöntemi ile hidrojen üretiminde çeşitli parametrelerin etkisinin incelenmesi. Gazi Univ J Sci Part C: Des Technol 7:957–968. https://doi.org/10.29109/gujsc.601223
11. Cigolotti V, Genovese M, Fragiacomo P (2021) Comprehensive review on fuel cell technology for stationary applications as sustainable and efficient poly-generation energy systems. Energies 14:4963. https://doi.org/10.3390/en14164963
12. Felseghi R-A, Carcadea E, Raboaca MS, Trufin CN, Filote C (2019) Hydrogen fuel cell technology for the sustainable future of stationary applications. Energies 12:4593. https://doi.org/10.3390/en12234593
13. Jin Y, Wang T, Che X, Dong J, Liu R, Yang J (2022) New high-performance bulky N-heterocyclic group functionalized poly(terphenyl piperidinium) membranes for HT-PEMFC applications. J Membr Sci 641:119884. https://doi.org/10.1016/j.memsci.2021.119884
14. Pang Y, Duan Y, Li Q, Liu B, Hu X, Liu Q, Zhao C (2023) Immobilized hindered amine radical scavenger for durability enhancement of perfluorosulfonic acid membrane in PEMFCs. J Membr Sci 686:121999. https://doi.org/10.1016/j.memsci.2023.121999
15. Wang Y, Xie Z, Zhang W, Liu H, Xu Q, Khotseng L, Su H (2023) Dual-functional phosphoric acid-loaded covalent organic framework for PEMFC self-humidification: optimization on membrane electrode assembly. Int J Hydrog Energy 48:32068–32076. https://doi.org/10.1016/j.ijhydene.2023.05.022
16. Haque MA, Sulong AB, Shyuan LK, Majlan EH, Husaini T, Rosli RE (2021) Synthesis of polymer/MWCNT nanocomposite catalyst supporting materials for high-temperature PEM fuel cells. Int J Hydrog Energy 46:4339–4353. https://doi.org/10.1016/j.ijhydene.2020.10.200
17. Nikouei MA, Oroujzadeh M, Mehdipour-Ataei S (2017) The PROMETHEE multiple criteria decision making analysis for selecting the best membrane prepared from sulfonated poly (ether ketone) s and poly (ether sulfone) s for proton exchange membrane fuel cell. Energy 119:77–85. https://doi.org/10.1016/j.energy.2016.12.052
18. Sahin A (2018) The development of Speek/Pva/Teos blend membrane for proton exchange membrane fuel cells. Electrochim Acta 271:127–136. https://doi.org/10.1016/j.electacta.2018.03.145
19. Baroutaji A, Carton J, Sajjia M, Olabi AG (2015) Materials in PEM fuel cells
20. Tellez-Cruz MM, Escorihuela J, Solorza-Feria O, Compañ V (2021) Proton exchange membrane fuel cells (PEMFCs): advances and challenges. Polymers 13:3064. https://doi.org/10.3390/polym13183064
21. Pollet B, Franco AA, Su H, Liang H, Pasupathi S (2016) Proton exchange membrane fuel cells, compendium of Hydrogen Energy, Elsevier, Amsterdam, pp. 3–56. https://doi.org/10.1016/B978-1-78242-363-8.00001-3
22. Peighambardoust SJ, Rowshanzamir S, Amjadi M (2010) Review of the proton exchange membranes for fuel cell applications. Int J Hydrog Energy 35:9349–9384. https://doi.org/10.1016/j.ijhydene.2010.05.017
23. Haque MA, Sulong A, Loh K, Majlan EH, Husaini T, Rosli RE (2017) Acid doped polybenzimidazoles based membrane electrode assembly for high temperature proton exchange membrane fuel cell: a review. Int J Hydrog Energy 42:9156–9179. https://doi.org/10.1016/j.ijhydene.2016.03.086
24. Şahin A, Ar İ (2015) Synthesis, characterization and fuel cell performance tests of boric acid and boron phosphate doped, sulphonated and phosphonated poly (vinyl alcohol) based composite membranes. J Power Sources 288:426–433. https://doi.org/10.1016/j.jpowsour.2015.03.188
25. Parekh A (2022) Recent developments of proton exchange membranes for PEMFC: a review. Front Energy Res 10:956132. https://doi.org/10.3389/fenrg.2022.956132
26. Esmaeili N, Gray EM, Webb CJ (2019) Non-fluorinated polymer composite proton exchange membranes for fuel cell applications–A review. ChemPhysChem 20:2016–2053. https://doi.org/10.1002/cphc.201900191
27. Walkowiak-Kulikowska J, Wolska J, Koroniak H (2017) Polymers application in proton exchange membranes for fuel cells (PEMFCs). Phys Sci Reviews 2:20170018. https://doi.org/10.1515/psr-2017-0018
28. Daud SNSS, Norddin MM, Jaafar J, Sudirman R, Othman M, Ismail A (2021) Highly sulfonated poly (ether ether ketone) blend with hydrophobic polyether sulfone as an alternative electrolyte for proton exchange membrane fuel cell. Arab J Sci Eng 46:6189–6205. https://doi.org/10.1007/s13369-020-04898-5
29. Çalı A, Şahin A, Ar İ (2022) Experimental investigation of boron phosphate Incorporated speek/pvdf blend membrane for proton exchange membrane fuel cells. Int J Hydrog Energy 47:40476–40490. https://doi.org/10.1016/j.ijhydene.2022.05.171
30. Poongan A, Kesava M, Mandal A, Murugan E (2023) Effect of ZrO2 nanoparticles on phosphoric acid-doped poly (Ethylene imine)/Polyvinyl alcohol) membrane for medium-temperature polymer electrolyte membrane fuel cell applications. Int J Hydrog Energy 48:27371–27382. https://doi.org/10.1016/j.ijhydene.2023.03.418
31. Kulasekaran P, Mahimai BM, Deivanayagam P (2020) Novel cross-linked poly (vinyl alcohol)-based electrolyte membranes for fuel cell applications. RSC Adv 10:26521–26527. https://doi.org/10.1039/D0RA04360E
32. Li X, Wang S, Zhang H, Lin C, Xie X, Hu C, Tian R (2021) Sulfonated poly(arylene ether sulfone)s membranes with distinct microphase-separated morphology for PEMFCs. Int J Hydrog Energy 46:33978–33990. https://doi.org/10.1016/j.ijhydene.2021.07.199

33. Haragirimana A, Ingabire PB, Zhu Y, Lu Y, Li N, Hu Z, Chen S (2019) Four-polymer blend proton exchange membranes derived from sulfonated poly(aryl ether sulfone)s with various sulfonation degrees for application in fuel cells. J Membr Sci 583:209–219. https://doi.org/10.1016/j.memsci.2019.04.014
34. Eskitoros-Togay ŞM, Bulbul YE, Cınar ZK, Sahin A, Dilsiz N (2023) Fabrication of PVP/sulfonated PES electrospun membranes decorated by sulfonated halloysite nanotubes via electrospinning method and enhanced performance of proton exchange membrane fuel cells. Int J Hydrog Energy 48:280–290. https://doi.org/10.1016/j.ijhydene.2022.09.214
35. Muliawati EC, Santoso M, Ismail AF, Jaafar J, Salleh MT, Nurherdiana SD, Widiastuti N (2017) Poly (Eugenol Sulfonate)-Sulfonated polyetherimide new blends membrane promising for direct methanol fuel cell. Malaysian J Anal Sci 21:659–668. https://doi.org/10.17576/mjas-2017-2103-15
36. Akay RG, Ata KC, Kadıoğlu T, Çelik C (2018) Evaluation of SPEEK/PBI blend membranes for possible direct borohydride fuel cell (DBFC) application. Int J Hydrog Energy 43:18702–18711. https://doi.org/10.1016/j.ijhydene.2018.07.129
37. Yang J, Li X, Shi C, Liu B, Cao K, Shan C, Hu W, Liu B (2021) Fabrication of PBI/SPOSS hybrid high-temperature proton exchange membranes using SPAEK as compatibilizer. J Membr Sci 620:118855. https://doi.org/10.1016/j.memsci.2020.118855
38. Gokulakrishnan SA, Kumar V, Arthanareeswaran G, Ismail AF, Jaafar J (2022) Thermally stable nanoclay and functionalized graphene oxide integrated SPEEK nanocomposite membranes for direct methanol fuel cell application. Fuel 329:125407. https://doi.org/10.1016/j.fuel.2022.125407
39. Harameen HMA, Akay RG (2023) Investigation into the influence of boron nitride addition on the properties of SPEEK/PBI based electrolyte membrane. Int J Hydrog Energy. https://doi.org/10.1016/j.ijhydene.2022.12.359
40. Yagizatli Y, Sahin A, Ar I (2022) Effect of thermal crosslinking process on membrane structure and PEM fuel cell applications performed with SPEEK-PVA blend membranes. Int J Hydrog Energy 47:40445–40461. https://doi.org/10.1016/j.ijhydene.2022.04.183
41. Rahmati M, Jangali M, Rezaei H (2019) An investigation of proton conductivity of PVA, PBI and SPEEK Polymer membranes using molecular dynamics simulation. J Mol Liq 296:111781. https://doi.org/10.1016/j.molliq.2019.111781
42. Sharma S, Prakash J, Pujari P (2015) Effects of the molecular level dispersion of graphene oxide on the free volume characteristics of poly (vinyl alcohol) and its impact on the thermal and mechanical properties of their nanocomposites. Phys Chem Chem Phys 17:29201–29209. https://doi.org/10.1039/C5CP05278E
43. Jabrail FH, Ahmad AZ, Gupta KC (2016) Synthesis and characterization of pH responsive polyvinyl alcohol hydrogels with chitosan and polyacrylonitrile. J Polym Mater 33:539
44. Yu J, Cheng S, Che Q (2017) Preparation and characterization of layer-by-layer self-assembly membrane based on sulfonated polyetheretherketone and polyurethane for high-temperature proton exchange membrane. J Polym Sci Part A: Polym Chem 55:3446–3454. https://doi.org/10.1002/pola.28725
45. Zhong S, Fu T, Dou Z, Zhao C, Na H (2006) Preparation and evaluation of a proton exchange membrane based on crosslinkable sulfonated poly (ether ether ketone) s. J Power Sources 162:51–57. https://doi.org/10.1016/j.jpowsour.2006.06.067
46. Rambabu G, Bhat SD (2018) Amino acid functionalized graphene oxide based nanocomposite membrane electrolytes for direct methanol fuel cells. J Membr Sci 551:1–11. https://doi.org/10.1016/j.memsci.2018.01.026
47. Maegawa K, Nagai H, Kumar R, Abdel-Galeil MM, Tan WK, Matsuda A (2023) Development of polybenzimidazole modification with open-edges/porous-reduced graphene oxide composite membranes for excellent stability and improved PEM fuel cell performance. Mater Chem Phys 294:126994. https://doi.org/10.1016/j.matchemphys.2022.126994
48. Yagizatli Y, Ulas B, Cali A, Sahin A, Ar I (2020) Improved fuel cell properties of Nano-TiO2 doped Poly (Vinylidene fluoride) and phosphonated poly (vinyl alcohol) composite blend membranes for PEM fuel cells. Int J Hydrog Energy 45:35130–35138. https://doi.org/10.1016/j.ijhydene.2020.02.197
49. Park C, Lee E, Lee G, Tak Y (2020) Superior durability and stability of pt electrocatalyst on N-doped graphene-TiO2 hybrid material for oxygen reduction reaction and polymer electrolyte membrane fuel cells. Appl Catal B 268:118414. https://doi.org/10.1016/j.apcatb.2019.118414
50. Seo K, Seo J, Nam KH, Han H (2017) Polybenzimidazole/inorganic composite membrane with advanced performance for high temperature polymer electrolyte membrane fuel cells. Polym Compos 38:87–95. https://doi.org/10.1002/pc.23563
51. Di S, Yan L, Han S, Yue B, Feng Q, Xie L, Chen J, Zhang D, Sun C (2012) Enhancing the high-temperature proton conductivity of phosphoric acid doped poly (2, 5-benzimidazole) by preblending boron phosphate nanoparticles to the raw materials. J Power Sources 211:161–168. https://doi.org/10.1016/j.jpowsour.2012.03.091
52. Hu H, Ding F, Ding H, Liu J, Xiao M, Meng Y, Sun L (2020) Sulfonated poly (fluorenyl ether ketone)/Sulfonated α-zirconium phosphate nanocomposite membranes for proton exchange membrane fuel cells. Adv Compos Hybrid Mater 3:498–507. https://doi.org/10.1007/s42114-020-00182-0
53. Al-Othman A, Nancarrow P, Tawalbeh M, Ka'ki A, El-Ahwal K, El Taher B, Alkasrawi M (2021) Novel composite membrane based on zirconium phosphate-ionic liquids for high temperature PEM fuel cells. Int J Hydrog Energy 46:6100–6109. https://doi.org/10.1016/j.ijhydene.2020.02.112
54. Ketpang K, Son B, Lee D, Shanmugam S (2015) Porous zirconium oxide nanotube modified Nafion composite membrane for polymer electrolyte membrane fuel cells operated under dry conditions. J Membr Sci 488:154–165. https://doi.org/10.1016/j.memsci.2015.03.096
55. Parnian MJ, Rowshanzamir S, Moghaddam JA (2018) Investigation of physicochemical and electrochemical properties of recast nafion nanocomposite membranes using different loading of zirconia nanoparticles for proton exchange membrane fuel cell applications. Mater Sci Energy Technol 1:146–154. https://doi.org/10.1016/j.mset.2018.06.008
56. Jesuraj K, Manimuthu RP (2019) Preparation and characterization of hybrid chitosan/PEO–silica membrane doped with phosphotungstic acid for PEM fuel cell application. Polymer-Plastics Technol Mater 58:14–30. https://doi.org/10.1080/03602559.2018.1455862
57. Wang X, Jin M, Li Y, Zhao L (2017) The influence of various ionic liquids on the properties of SPEEK membrane doped with mesoporous silica. Electrochim Acta 257:290–300. https://doi.org/10.1016/j.electacta.2017.10.098
58. Nasef MM, Fujigaya T, Abouzari-Lotf E, Nakashima N, Yang Z (2016) Enhancement of performance of pyridine modified polybenzimidazole fuel cell membranes using zirconium oxide nanoclusters and optimized phosphoric acid doping level. Int J Hydrog Energy 41:6842–6854. https://doi.org/10.1016/j.ijhydene.2016.03.022
59. Li X, Wu X, Liu S, Li Y, Fan J, Lv K (2020) Effects of fluorine on photocatalysis. Chin J Catal 41:1451–1467. https://doi.org/10.1016/S1872-2067(20)63594-X
60. Ding B, Kim HY, Lee SC, Shao CL, Lee DR, Park SJ, Kwag GB, Choi KJ (2002) Preparation and characterization of a nanoscale poly (vinyl alcohol) fiber aggregate produced by

an electrospinning method. J Polym Sci Part B: Polym Phys 40:1261–1268. https://doi.org/10.1002/polb.10191
61. Reyes-Rodriguez J, Solorza-Feria O, García-Bernabé A, Giménez E, Sahuquillo O, Compañ V (2016) Conductivity of composite membrane-based poly (ether-ether-ketone) sulfonated (SPEEK) nanofiber mats of varying thickness. RSC Adv 6:56986–56999. https://doi.org/10.1039/C6RA08228A
62. Kim J-D, Donnadio A, Jun M-S, Di Vona ML (2013) Crosslinked SPES-SPPSU membranes for high temperature PEMFCs. Int J Hydrog Energy 38:1517–1523. https://doi.org/10.1016/j.ijhydene.2012.10.110
63. Salarizadeh P, Javanbakht M, Pourmahdian S, Hazer MSA, Hooshyari K, Askari MB (2019) Novel proton exchange membranes based on proton conductive sulfonated PAMPS/PSSA-TiO2 hybrid nanoparticles and sulfonated poly (ether ether ketone) for PEMFC. Int J Hydrog Energy 44:3099–3114. https://doi.org/10.1016/j.ijhydene.2018.11.235
64. Çalı A, Şahin A, Ar İ (2020) Incorporating sepiolite and kaolinite to improve the performance of SPEEK composite membranes for proton exchange membrane fuel cells. Can J Chem Eng 98:892–904. https://doi.org/10.1002/cjce.23681
65. Zhilov V, Kostikova G, Kuz´ mina L, Demina L, Demin S, Tsivadze AY (2018) Complexation of tetrafluoroboric acid with benzo-15-crown-5. Russ Chem Bull 67:2191–2194. https://doi.org/10.1007/s11172-018-2354-6
66. Leoni P, Sommovigo M, Pasquali M, Midollini S, Braga D, Sabatino P (1991) Coordinated water/anion hydrogen bonds and Pd-H bond acidity in cationic palladium (II) aquo hydrides and the x-ray crystal and molecular structures of trans-[(Cy3P) 2Pd (H) (H2O)] BF4 (Cy = cyclohexyl). Organometallics 10:1038–1044. https://doi.org/10.1016/S0016-7037(03)00096-6
67. Peak D, Luther IIIGW, Sparks DL (2003) ATR-FTIR spectroscopic studies of boric acid adsorption on hydrous ferric oxide. Geochim Cosmochim Acta 67:2551–2560. https://doi.org/10.1016/S0016-7037(03)00096-6
68. Su C, Suarez DL (1995) Coordination of adsorbed boron: a FTIR spectroscopic study. Environ Sci Technol 29:302–311
69. Song J-M, Shin J, Sohn J-Y, Nho YC (2011) Preparation and characterization of SPEEK membranes crosslinked by electron beam irradiation. Macromol Res 19:1082–1089. https://doi.org/10.1007/s13233-011-1013-7
70. Shashidhara G, Kumar KN (2010) Proton conductivity of SPEEK membranes. Polym-Plast Technol Eng 49:796–806. https://doi.org/10.1080/03602551003749601
71. Zeytuncu B, Morcali MH, Akman S, Yucel O (2015) Influence of polyvinyl alcohol amount on producing in situ photo-crosslinked thioamide functionalized nanofiber membranes. J Serb Chem Soc 80:97–106. https://doi.org/10.2298/JSC140317083Z
72. Aziz SB, Abdulwahid RT, Rasheed MA, Abdullah OG, Ahmed HM (2017) Polymer blending as a novel approach for tuning the SPR peaks of silver nanoparticles. Polymers 9:486. https://doi.org/10.3390/polym9100486
73. Gupta S, Pramanik AK, Kailath A, Mishra T, Guha A, Nayar S, Sinha A (2009) Composition dependent structural modulations in transparent poly (vinyl alcohol) hydrogels. Colloids Surf B 74:186–190. https://doi.org/10.1016/j.colsurfb.2009.07.015
74. Nangia R, Shukla NK, Sharma A (2018) Frequency and temperature-dependent impedance spectroscopy of PVA/PEG polymer blend film. High Perform Polym 30:918–926. https://doi.org/10.1177/0954008318774837
75. Sowmya G, Gowrishankar S, Ramesh Prabhu M (2020) Influence of phosphotungstic acid in sulfonated poly (ether ether ketone)/poly (amide imide) based Proton conductive membranes and its impact on the electrochemical studies of microbial fuel cell application. Ionics 26:1841–1852. https://doi.org/10.1007/s11581-019-03415-5
76. Parnian MJ, Rowshanzamir S, Gashoul F (2017) Comprehensive investigation of physicochemical and electrochemical properties of sulfonated poly (ether ether ketone) membranes with different degrees of sulfonation for proton exchange membrane fuel cell applications. Energy 125:614–628. https://doi.org/10.3390/en14164963
77. Salarizadeh P, Javanbakht M, Pourmahdian S (2017) Enhancing the performance of SPEEK Polymer electrolyte membranes using functionalized TiO 2 nanoparticles with proton hopping sites. RSC Adv 7:8303–8313. https://doi.org/10.1039/C6RA25959F
78. Sahin A, Tasdemir HM, Ar İ (2019) Improved performance and durability of sulfonated polyether ether ketone/cerium phosphate composite membrane for proton exchange membrane fuel cells. Ionics 25:5163–5175. https://doi.org/10.1007/s11581-019-03109-y
79. Venkatram S, Batra R, Chen L, Kim C, Shelton M, Ramprasad R (2020) Predicting crystallization tendency of polymers using multifidelity information fusion and machine learning. J Phys Chem B 124:6046–6054. https://doi.org/10.1021/acs.jpcb.0c01865
80. Konno H, Taylor LS (2006) Influence of different polymers on the crystallization tendency of molecularly dispersed amorphous felodipine. J Pharm Sci 95:2692–2705. https://doi.org/10.1002/jps.20697
81. Antonucci P, Arico A, Cretı P, Ramunni E, Antonucci V (1999) Investigation of a direct methanol fuel cell based on a composite Nafion®-silica electrolyte for high temperature operation. Solid State Ionics 125:431–437. https://doi.org/10.1016/S0167-2738(99)00206-4
82. Kim H, Lee S, Kim S, Oh C, Ryu J, Kim J, Park E, Hong S, No K (2017) Membrane crystallinity and fuel crossover in direct ethanol fuel cells with Nafion composite membranes containing phosphotungstic acid. J Mater Sci 52:2400–2412. https://doi.org/10.1007/s10853-016-0534-z
83. Liu D, Xie Y, Zhong J, Yang F, Pang J, Jiang Z (2022) High methanol resistance semi-crystalline sulfonated poly(ether ketone) proton exchange membrane for direct methanol fuel cell. J Membr Sci 650:120413. https://doi.org/10.1016/j.memsci.2022.120413
84. Shao Z-G, Joghee P, Hsing IM (2004) Preparation and characterization of hybrid nafion–silica membrane doped with phosphotungstic acid for high temperature operation of proton exchange membrane fuel cells. J Membr Sci 229:43–51. https://doi.org/10.1016/j.memsci.2003.09.014
85. Kim YB, Gür TM, Jung H-J, Kang S, Sinclair R, Prinz FB (2011) Effect of crystallinity on proton conductivity in yttrium-doped barium zirconate thin films. Solid State Ionics 198:39–46. https://doi.org/10.1016/j.ssi.2011.07.004
86. Tang H, Lv X, Du J, Liu Y, Liu J, Guo L, Zheng X, Hao H, Liu Z (2022) Improving proton conductivity of metal organic framework materials by reducing crystallinity. Appl Organomet Chem 36:e6777. https://doi.org/10.1002/aoc.6777
87. Yin C, Wang Z, Luo Y, Li J, Zhou Y, Zhang X, Zhang H, Fang P, He C (2018) Thermal annealing on free volumes, crystallinity and proton conductivity of Nafion membranes. J Phys Chem Solids 120:71–78. https://doi.org/10.1016/j.jpcs.2018.04.028
88. Escorihuela J, Narducci R, Compañ V, Costantino F (2019) Proton conductivity of composite polyelectrolyte membranes with metal-organic frameworks for fuel cell applications. Adv Mater Interfaces 6:1801146. https://doi.org/10.1002/admi.201801146
89. Pu H, Wang L, Pan H, Wan D (2010) Synthesis and characterization of fluorine-containing polybenzimidazole for proton conducting membranes in fuel cells. J Polym Sci Part A: Polym Chem 48:2115–2122. https://doi.org/10.1002/pola.23979

90. Yang T (2008) Preliminary study of SPEEK/PVA blend membranes for DMFC applications. Int J Hydrog Energy 33:6772–6779. https://doi.org/10.1016/j.ijhydene.2008.08.022
91. Jun M-S, Choi Y-W, Kim J-D (2012) Solvent casting effects of sulfonated poly (ether ether ketone) for polymer electrolyte membrane fuel cell. J Membr Sci 396:32–37. https://doi.org/10.1016/j.memsci.2011.12.008
92. Shakshooki S, Najeh-Ali B, Rais S, Hamassi A (2014) Poly (vinylalcohol)/Lamellar germanium phosphate nanocomposite membranes. Int J Sci Technol 3
93. Knauth P, Hou H, Bloch E, Sgreccia E, Di Vona M (2011) Thermogravimetric analysis of SPEEK membranes: thermal stability, degree of sulfonation and cross-linking reaction. J Anal Appl Pyrol 92:361–365. https://doi.org/10.1016/j.jaap.2011.07.012
94. Hou H, Polini R, Di Vona ML, Liu X, Sgreccia E, Chailan J-F, Knauth P (2013) Thermal crosslinked and nanodiamond reinforced SPEEK composite membrane for PEMFC. Int J Hydrog Energy 38:3346–3351. https://doi.org/10.1016/j.ijhydene.2012.12.019
95. Yang C-C, Chien W-C, Li YJ (2010) Direct methanol fuel cell based on poly (vinyl alcohol)/titanium oxide nanotubes/poly (styrene sulfonic acid)(PVA/nt-TiO2/PSSA) composite polymer membrane. J Power Sources 195:3407–3415. https://doi.org/10.1016/j.jpowsour.2009.12.024
96. Yang X, Zhang C, Wu L (2015) Nano γ-Fe_2O_3-supported fluoroboric acid: a novel magnetically recyclable catalyst for the synthesis of 12-substituted-benzo [h][1, 3] dioxolo [4, 5-b]-acridine-10, 11-diones as potent antitumor agents. RSC Adv 5:25115–25124. https://doi.org/10.1039/C5RA00887E
97. Toft M (2012) The effect of crystalline morphology on the glass transition and enthalpic relaxation in poly (ether-ether-ketone). University of Birmingham, Birmingham
98. Askadskii AA, Popova M, Matseevich T, Kurskaya E (2014) The influence of the degree of crystallinity on the glass transition temperature of polymers. Adv Mater Res 864:751–754. https://doi.org/10.4028/www.scientific.net/AMR.864-867.751
99. Li Y, Cui J, Li C, Zhou H, Chang J, Aras O, An F (2022) 19F MRI nanotheranostics for Cancer Management. Progress and Prospects ChemMedChem 17:e202100701. https://doi.org/10.1002/cmdc.202100701
100. Mertens M, Mohr M, Bruehne K, Fecht H-J, Łojkowski M, Święszkowski W, Łojkowski W (2016) Patterned hydrophobic and hydrophilic surfaces of ultra-smooth nanocrystalline diamond layers. Appl Surf Sci 390:526–530. https://doi.org/10.1016/j.apsusc.2016.08.130
101. Kavesh S, Schultz J (1969) Meaning and measurement of crystallinity in polymers: a review. Polym Eng Sci 9:331–338. https://doi.org/10.1002/pen.760090504
102. Negoro T, Thodsaratpreeyakul W, Takada Y, Thumsorn S, Inoya H, Hamada H (2016) Role of crystallinity on moisture absorption and mechanical performance of recycled PET compounds. Energy Procedia 89:323–327. https://doi.org/10.1016/j.egypro.2016.05.042
103. Harrison KL, Jenkins MJ (2004) The effect of crystallinity and water absorption on the dynamic mechanical relaxation behaviour of polycaprolactone. Polym Int 53:1298–1304. https://doi.org/10.1002/pi.1517
104. Subianto S, Pica M, Casciola M, Cojocaru P, Merlo L, Hards G, Jones DJ (2013) Physical and chemical modification routes leading to improved mechanical properties of perfluorosulfonic acid membranes for PEM fuel cells. J Power Sources 233:216–230. https://doi.org/10.1016/j.jpowsour.2012.12.121
105. Hamrock SJ, Yandrasits MA (2006) Proton exchange membranes for fuel cell applications. J Macromol Sci Part C: Polym Rev 46:219–244. https://doi.org/10.1080/15583720600796474
106. Tang Y, Kusoglu A, Karlsson AM, Santare MH, Cleghorn S, Johnson WB (2008) Mechanical properties of a reinforced composite polymer electrolyte membrane and its simulated performance in PEM fuel cells. J Power Sources 175:817–825. https://doi.org/10.1016/j.jpowsour.2007.09.093
107. Rynkowska E, Fatyeyeva K, Marais S, Kujawa J, Kujawski W (2019) Chemically and thermally crosslinked PVA-based membranes: effect on swelling and transport behavior. Polymers 11:1799. https://doi.org/10.3390/polym11111799
108. Deshmukh A, Wadaskar P, Malpe D (1995) Fluorine in environment: a review. Gondwana Geol Mag 9:1–20
109. Murmu R, Roy D, Patra SC, Sutar H, Senapati P (2022) Preparation and characterization of the SPEEK/PVA/Silica hybrid membrane for direct methanol fuel cell (DMFC). Polym Bull 79:2061–2087. https://doi.org/10.1007/s00289-021-03602-3
110. Reyes-Rodriguez JL, Escorihuela J, García-Bernabé A, Giménez E, Solorza-Feria O, Compañ V (2017) Proton conducting electrospun sulfonated polyether ether ketone graphene oxide composite membranes. RSC Adv 7:53481–53491. https://doi.org/10.1039/C7RA10484G
111. Yoon SI, Ma KY, Kim T-Y, Shin HS (2021) Correction: Proton conductivity of a hexagonal boron nitride membrane and its energy applications. J Mater Chem A 9:2470–2470. https://doi.org/10.1039/D1TA90007B
112. Wang L, Yi B, Zhang H, Liu Y, Xing D, Shao Z-G, Cai Y (2007) Sulfonated polyimide/PTFE reinforced membrane for PEMFCs. J Power Sources 167:47–52. https://doi.org/10.1016/j.jpowsour.2006.12.111
113. Haragirimana A, Li N, Hu Z, Chen S (2021) A facile, effective thermal crosslinking to balance stability and proton conduction for proton exchange membranes based on blend sulfonated poly (ether ether ketone)/sulfonated poly (arylene ether sulfone). Int J Hydrog Energy 46:15866–15877. https://doi.org/10.1016/j.ijhydene.2021.02.022
114. Park CH, Lee CH, Guiver MD, Lee YM (2011) Sulfonated hydrocarbon membranes for medium-temperature and low-humidity proton exchange membrane fuel cells (PEMFCs). Prog Polym Sci 36:1443–1498. https://doi.org/10.1016/j.progpolymsci.2011.06.001
115. Parnian MJ, Gashoul F, Rowshanzamir S (2017) Studies on the SPEEK membrane with low degree of sulfonation as a stable proton exchange membrane for fuel cell applications. Hydrog Fuel Cell Energy Storage 3:221–232. https://doi.org/10.22104/IJHFC.2017.428
116. Akbarian-Feizi L, Mehdipour-Ataei S, Yeganeh H (2010) Survey of sulfonated polyimide membrane as a good candidate for nafion substitution in fuel cell. Int J Hydrog Energy 35:9385–9397. https://doi.org/10.1016/j.ijhydene.2010.03.072
117. Tamura T, Kawakami H (2010) Aligned electrospun nanofiber composite membranes for fuel cell electrolytes. Nano Lett 10:1324–1328. https://doi.org/10.1021/nl1007079
118. Gao C, Chen J, Zhang B, Wang L (2020) Effect of chemical structure and degree of branching on the stability of proton exchange membranes based on sulfonated polynaphthylimides. Polymers 12:652. https://doi.org/10.3390/polym12030652
119. Altaf F, Batool R, Gill R, Rehman ZU, Majeed H, Ahmad A, Shafiq M, Dastan D, Abbas G, Jacob K (2021) Synthesis and electrochemical investigations of ABPBI grafted montmorillonite based Polymer electrolyte membranes for PEMFC applications. Renew Energy 164:709–728. https://doi.org/10.1016/j.renene.2020.09.104